Version of Record: https://www.sciencedirect.com/science/article/pii/S0377042721006208
Manuscript_d496ce70c07f8597b06a77783cf28fee

Vapor-liquid equilibrium estimation of n-alkane/nitrogen mixtures using neural networks

Suman Chakraborty[1*], Yixuan Sun[2*], Guang Lin[2,3], Li Qiao[1]

[1]School of Aeronautics and Astronautics, Purdue University, West Lafayette, IN 47907, USA

[2]School of Mechanical Engineering, Purdue University, West Lafayette, IN 47907, USA

[3]Department of Mathematics, Purdue University, West Lafayette, IN 47907, USA

Abstract

Understanding fluid phase behavior, like VLE, in high P&T conditions is crucial for developing high-fidelity simulations of chemically reacting flows in liquid-fueled combustion systems and also forms an integral part of the design-modeling of the control processes in chemical industries. Two data-driven models have been proposed in this study, each of which was competent in estimating VLE for the Type III binary systems of C_{10}/N_2 and C_{12}/N_2, at pressures ranging up to 50-60 MPa. Both models showed better performance in predicting equilibrium pressure as compared to VLE modeled using PR-EOS. A modified model has also been proposed, capable of estimating the full phase envelope for the binary systems of C_{10}/N_2 and C_{12}/N_2 across a wide range of temperatures, and thus exhibit the mixture critical pressure at the concerned temperature. The diverse applicability of the proposed network architecture was further exhibited while estimating the VLE of a ternary system of $C_1/C_{10}/N_2$.

Keywords: vapor-liquid equilibrium (VLE), neural networks, data-driven learning, Peng Robinson equation of state (PR-EOS), binary mixtures, ternary mixtures, critical locus, mixture critical point

1. Introduction

Phase equilibrium calculations play a crucial role in the study of high-pressure liquid fuel injection processes, involving some complex physical processes such as mixing, atomization, and evaporation [1–4]. Understanding of phase equilibrium behavior, specifically, vapor-liquid equilibrium (VLE) forms an important premise in the design of distillation processes, widely used in the chemical industry [5]. Even in the oil and gas sector, VLE behavior of nitrogen/alkane systems helps to understand nitrogen solubility, which in turn can be utilized in designing the nitrogen injection systems used for oil recovery [6]. The design and optimization of the control facilities of the aforementioned applications heavily rely on VLE data.

Binary mixtures of n-alkanes/nitrogen, except for methane, follow a Type III phase behavior according to the works of Scott and van Konynenburg [7]. The discontinuous critical line phase behavior exhibited by Type III mixtures poses challenges in its theoretical prediction [8,9]. One part of the critical locus, starts at the critical point of the heavier species and rises up to infinitely high pressures, whereas the other starts at the critical point of the lighter species and ends up meeting a three-phase vapor–liquid-liquid equilibrium (VLLE) coexistence line. Several experimental studies [10–16] have reported the vapor-liquid equilibrium behavior of n-alkane/nitrogen binary systems. However, the experimental database of VLE data for heavy n-alkane/nitrogen mixtures is scanty, with very few studies on heavier alkanes and even fewer in the high pressure and temperature range [6,17].

VLE modeling using the equation of state (EOS) is another way to study the phase behavior of n-alkane/nitrogen systems. The Peng–Robison equation of state (PR-EOS) [18] is one of the more popular EOS models for heavier alkanes [19]. However, there is a downside to using the EOS models. Firstly, the equation of states involves empirical parameters, especially for mixing rules which require a binary interaction parameter (BIP) for the accurate modeling of VLE using EOS, which is hard to determine [20]. Some studies proposed a constant BIP for a mixture system by minimizing the difference between experimental and EOS modeled pressures and vapor compositions [6,17]. Fateen et al. [20] proposed a semi-empirical relation for BIP based on Huron-Vidal mixing rules, for over 60 binary mixtures, which also allowed the BIP to exhibit unsymmetrical behavior. Some studies [21,22] have proposed generalized BIP correlations to be used with PR-EOS, making use of limited experimental data in the literature [20]. Another issue of VLE modeling using EOS is the iterative nature of the process, which can cause delays for real-time, on-the-fly calculations in an industrial application [23].

Development in the fields of data-driven (DD) learning and neural networks (NN) offer a fast and computationally efficient alternative to solving VLE problems [23–32]. Neural networks have also been used in estimating other thermodynamic and transport properties of mixtures [33–37]. NNs are capable of capturing the non-linear and complex patterns between a set of parameters, without any prior knowledge of the governing equations or physics of the problem. For a VLE problem, a network can be trained to predict the non-linear mapping between the equilibrium temperature (T), pressure (P) and composition (x, y) in the liquid and vapor phase [25]. The study by Sharma et al. [25] explored the use of a backpropagation algorithm in the VLE prediction of methane/ethane and ammonia/water systems and found the results to be within $\pm 1\%$ accuracy. Urata et al. [38] used an artificial neural network (ANN) to predict the VLE behavior of binary mixtures consisting of hydrofluoroethers (HFEs) and polar compounds. Mohanty [23,27] also used ANN to study VLE for the binary systems of carbon dioxide/difluoromethane, ethyl caproate, ethyl caprylate, and ethyl caprate, the likes of which are either used as refrigerants or are significant in supercritical extraction. A Least Squares Support Vector Machine (LSSVM) model, with a R^2 of 0.9932, was used by Mesbah et al. [39] in predicting the phase behavior of 7 carbon dioxide/hydrocarbon binary mixtures. In a more recent study by Roosta et al. [40], ANN was used to predict the VLE of methane to n-heptane binary mixtures and proposed closed-form expressions using genetic programming.

Motivated by the above, this study uses data-driven models for predicting the VLE of two mixtures: n-decane/nitrogen (C_{10}/N_2) and n-dodecane/nitrogen (C_{12}/N_2), at pressures up to 50–60 MPa. The data-driven models formulated as a part of this study have been made with the goals of:

I. To bypass the need for estimating and/or formulating a binary interaction parameter. The process and experimental data required for the same are either non-existent or hard to acquire
II. A model that can be trained on the minimal experimental data points available, and is still able to capture the vapor-liquid equilibrium behavior at high temperatures and pressures

Keeping the goals in mind, two different data-driven unified models were proposed. The first model (DD-Int) was trained based on an interpolated data set generated from the experimental data and worked for both binary mixtures. The second unified model (DD-Ind-T) has been trained using the data generated from individual sub-models, which were trained on temperature-specific (isotherm) VLE data. The equilibrium pressure (P) and vapor phase mole fraction (y) predicted using the data-driven models were then compared with the experimental data and PR-EOS modeled data. An improved version of the DD-Ind-T model (v2) was also trained using the additional feature of the critical locus data of the binary systems of C_{10}/N_2 and C_{12}/N_2. The network architecture was also trained to predict the equilibrium pressure and vapor mole fractions of a ternary system of methane/n-decane/nitrogen ($C_1/C_{10}/N_2$).

2. Neural Network Theory

Inspired by nature, neural networks, especially deep neural networks have been widely used in solving data-driven problems in recent years. The universal approximation theorem [41] states that it is possible to represent any function using a simple feed-forward neural network with only a single hidden layer. Neural networks have been trained to model a wide range of functions in an input-output paired supervised way as they are powerful function approximators. The development of deep learning techniques overcame the problem that the number of nodes in a single-layered neural network can be infeasibly large when approximating complex functions. Gradient-based optimization methods, backpropagation [42], and high-performance computing made it possible to efficiently train very deep neural networks.

Deep neural networks have been making major advances in solving various engineering problems, such as mechanical properties prediction of porous media [43,44], outage prediction and deriving generation dispatch in power grids [45,46], and material temperature measurement and crack detection based on infrared thermography [47,48]. In this work, we mainly focus on a basic form of neural network - feedforward fully connected networks to inspect their ability to model the VLE of Type III binary mixtures, involving long-chain n-alkanes, at different temperatures with limited experimental data. Feedforward networks comprise an input layer, several hidden layers, and an output layer. In general, the feedforward fully connected networks take the input information at the input layer and then pass it to each node in the subsequent layer, which can be described as:

$$\boldsymbol{Y} = \boldsymbol{X}\,\boldsymbol{W} + \boldsymbol{b} \qquad (3.1)$$

where $\boldsymbol{X} \in \mathbb{R}^{n \times m}$ is the input matrix containing n data points and m features; $\boldsymbol{W} \in \mathbb{R}^{m \times h}$ is the weight matrix, in which h is the number of nodes in the subsequent layer; $\boldsymbol{b} \in \mathbb{R}^{h}$ is the bias vector. In this study, features are the mixture properties used for predicting the equilibrium pressure and vapor phase composition of N_2, such as mixture type, temperature, liquid phase composition of the mixture. At each node in the subsequent layer, an activation operation is implemented. It introduces non-linearity into the network, enabling it to capture the non-linear relations between the input information and the output. The final output from the subsequent layer is:

$$\mathbf{O} = a(\boldsymbol{Y}) = a(\boldsymbol{X}\,\boldsymbol{W} + \boldsymbol{b}) \qquad (3.2)$$

where $a(\cdot)$ is the activation function, which is usually a non-linear and differentiable function. The output of the current layer becomes the input to the next subsequent layer and the same process is repeated until the output layer. The value from the network's output layer can be compared with the real value, given the input, using a suitable loss function. Gradient-based optimization methods with backpropagation can help search for the optimal weights that minimize the loss.

3. Learning Scheme

In this section, we introduce the process of data augmentation, the choice and implementation of deep learning models, and the evaluation metrics used for measuring model performance. Three different neural network architectures were used in this work.

3.1 Data Augmentation

Training an effective deep neural network requires adequate data, especially when the network is complex. Due to the fact that the experimental data for each temperature only contained about 15 – 27 data points, augmenting the experimental data for model training was necessary. Two augmentation methods, linear interpolation and data generation from individually trained temperature-dependent models were adopted in this work to enlarge the training dataset size. The augmented data were used to train a model that took temperature (T), liquid phase composition of the mixture (x_1, x_2) as inputs, and then output equilibrium pressure (P) and vapor composition of N_2 (y_1). From this point onward, N_2 will be referred to as component – 1 (x_1, y_1) and the n-alkanes as component – 2 (x_2, y_2).

3.1.1 Linear Interpolation

Despite being simple, interpolating samples in feature space is a useful way to augment the dataset, which is able to effectively reduce model overfitting. Consider an experimental dataset having N_{exp} points, thus having $(N_{exp} - 1)$ data slots. The goal is to generate N_{inter} new points using interpolation, such that each of the experimental data slots will house $N_{new-eachslot} = \left({N_{inter}}/{N_{exp} - 1} \right)$ points. For a particular isotherm, for every two experimental data points of x, y and P, $N_{new-eachslot}$ number of new points were inserted. The new points were generated using section formula as follows:

$$x_{new} = \frac{\left(fact1 \times x_{exp,i+1}\right) + \left(fact2 \times x_{exp,i}\right)}{fact1 + fact2} \tag{3.1}$$

where, $x_{exp,i}$ and $x_{exp,i+1}$ are two consecutive experimental data points between which the new points were generated. The new point (x_{new}) divided the line segment joining the two experimental points in the ratio of $fact1$:$fact2$, where both $fact1$ and $fact2$ were positive integers and satisfied Eqn. 4.2. $fact1$ could take values between (1 + $N_{new-eachslot}$) and the corresponding value of $fact2$.

$$fact1 + fact2 = N_{new-eachslot} + 1 \tag{3.2}$$

3.1.2 Data Generation from Temperature – specific Models

Another approach to data augmentation was to generate data from individual models trained on specific temperatures. The experimental data contained a few samples at various temperatures. While the size of the dataset was not enough for a model that took the temperature as one of the features, training models conditioned on temperature led to good performance. That is, for each temperature in the experimental dataset, a neural network was trained only on the VLE profile of the mixture for that isotherm. And then the trained models were used to generate new data points by taking randomly sampled x_1 and x_2 values. Finally, the new data generated from those individual models conditioned on temperatures were used to train a single model that takes x_1, x_2 as well as the T as the input to predict y_1 and P.

3.2 Network Architecture

Based on the nature of the tabular format of the data, all three aforementioned architectures were fully connected feed-forward neural networks. A fully connected network comprises an input layer, an output layer, and several hidden layers, with nodes connected to each other between adjacent layers.

3.2.1 Temperature – specific, Single Composition Models

To address the dataset size problem, individual neural network models were adopted to generate VLE profile data conditioned on temperatures. In each individual network, the input layer had two nodes, taking x_1 and x_2, respectively, and the output layer contained 2 nodes, giving out y_1 and P. The architecture of the individual models is shown in Fig. 1.

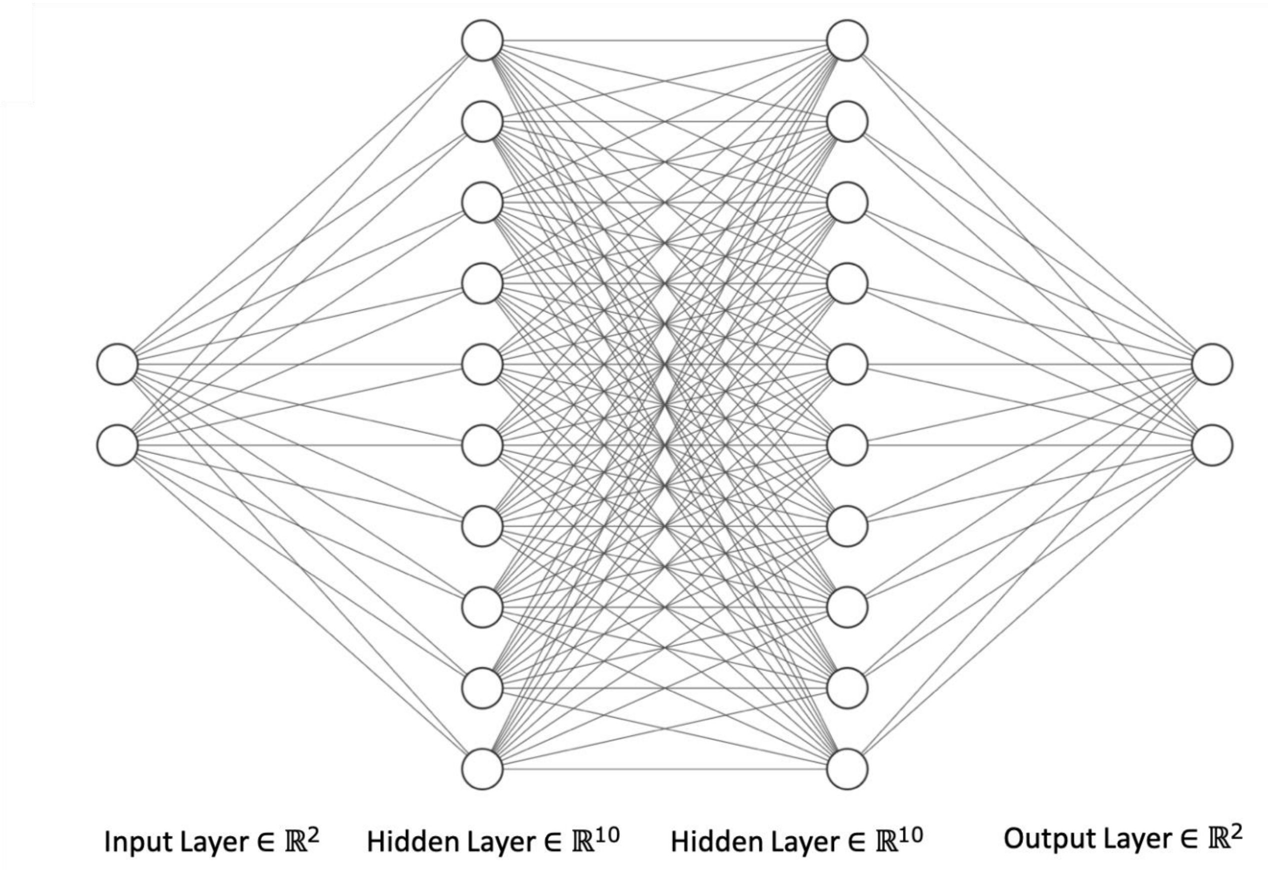

Fig. 1: Temperature–specific network architecture

A rectified linear unit (ReLU) activation function was placed at each node in the hidden layers, which introduces non-linearity to the network. From the last hidden layer to the output layer, a linear mapping was introduced so that the output values were not constrained by any activation to serve the purpose of regression.

3.2.2 Composition – specific Models

The augmented data were fed into a model that took T, x_1, and x_2 values of a specific binary mixture as the input to predict the corresponding y_1 and P. In the composition-specific model, there were 3 hidden layers with 10 nodes in each layer. While it had a similar structure with respect to the temperature-specific, single composition model, on the node for y_1 value in the output layer, a sigmoid activation was placed to constrain the output to [0, 1], shown in Fig. 2. The same architecture was used to train models for both the binary mixtures of C_{10}/N_2 and C_{12}/N_2.

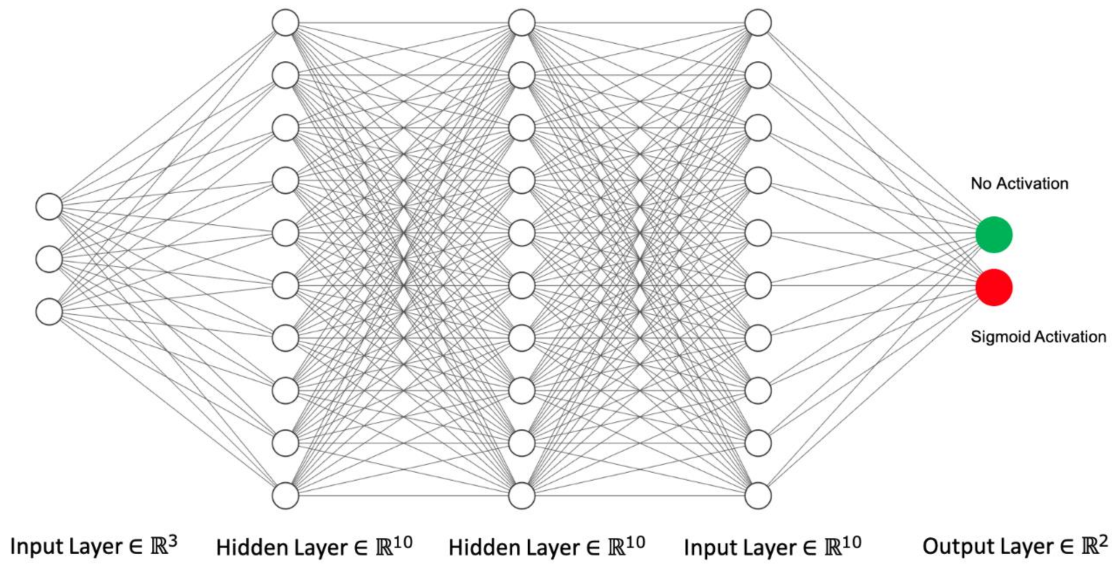

Fig. 2: Composition–specific model. The input layer takes x_1, x_2 values of a binary mixture, as well as the temperature. On the node for y_1 in the output layer, a sigmoid activation is used for constraining the output value.

3.2.3 Combined Composition Model

In addition, we explored deep neural networks' ability to model the VLE of more than one binary system. The combined composition model took x_1, x_2, T, and a model identifier that indicates whether it was a C_{10}/N_2 or C_{12}/N_2 system, as the input and then output the corresponding y_1 and P. This network had 4 nodes in the input layer and 4 hidden layers with 10 nodes in each. Similarly, a sigmoid activation was employed at the node giving out y_1 value in the output layer, shown in Fig 3.

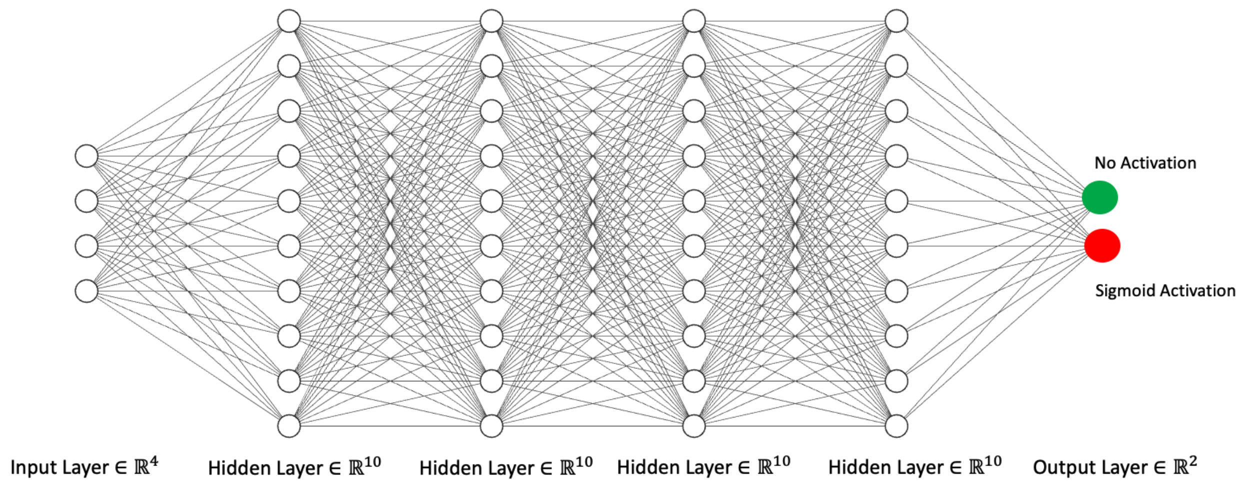

Fig. 3: Binary composition model. An additional binary feature, composition identifier, is fed in the network.

3.3 Evaluation Metrics

The metrics employed for evaluating model performance were the mean squared error (MSE) and coefficient of determination (R^2). MSE is a commonly used metric, also a loss function in training neural networks for regression problems. It indicates the average squared deviation between the predicted value and the true value. A lower mean squared error indicates that the model makes better predictions.

$$MSE = \frac{\sum_{i=1}^{N}\left(y_{pred} - y_{true}\right)^2}{N} \tag{3.3}$$

Equation 3.3 shows the definition of MSE, where N is the sample size, y_{pred} is the predicted value from the model and y_{true} is the true label value of the given sample.

A second metric used in this work was the coefficient of determination, R^2, which depicts the extent of the variance in the dependent variable that can be anticipated from the independent variables. The R^2 is defined as

$$R^2 = 1 - \frac{SS_{res}}{SS_{tot}} \tag{3.4}$$

where the residual sum of squares is $SS_{res} = \sum_{i=1}^{N}\left(y_{true} - y_{pred}\right)^2$, the total sum of squares is $SS_{tot} = \sum_{i=1}^{N}(y_{true} - \bar{y}_{true})^2$, and $\bar{y}_{true}$ is the average value of the true values. The values of R^2 are usually between 0 and 1. If we have a perfect model that can explain all the variance presented in the data, we will have R^2 score of 1.

Another metric used is the average absolute error (AAE) as shown in equation 3.5.

$$AAE = \frac{1}{N}\sum_{i=1}^{N}\frac{\left|P_{Exp} - P_{model}\right|}{P_{Exp}} \times 100 \tag{3.5}$$

where N is the number of data points, P_{Exp} is the equilibrium pressure from experimental data and P_{model} is the equilibrium pressure estimated either using PR-EOS model or the data-driven learning models.

3.4 Experimental Data and Data Setup for Learning

The experimental data used in this study for the binary systems of n-decane/nitrogen (C_{10}/N_2) and n-dodecane/nitrogen (C_{12}/N_2) were taken from the works of Garcia-Sanchez et al. [6] and Garcia-Cordova et al. [17] respectively. The critical temperatures and pressures for nitrogen, n-decane and n-dodecane are [126.19, 617.8, 658.2] K and [33.97, 21.1, 18] bar respectively [49]. For each of the two mixtures, the machine learning models were trained on isotherm data which lied between the critical temperatures of the individual components. A summary of the data set size used for each isotherm, for the two mixtures, is presented in Table 1.

Table 1: Summary of VLE Experimental Data Set

Mixture	Temperature [K]	No. of points	Source
C_{10}/N_2	344.6	23	Garcia-Sanchez et al. [6]
	377.4	22	
	410.9	23	
	463.7	23	
	503	20	
	533.5	17	
	563.1	14	
C_{12}/N_2	344.4	25	Garcia-Cordova et al. [17]
	410.7	27	

	463.9	27	
	503.4	27	
	532.9	25	
	562.1	23	
	593.5	15	

To examine model performance on different training and validation sets, the training of the networks was done via 10-fold cross-validation. In this process, the original data were randomly split into 10 subsets with equal sizes. For each training cycle, nine of the subsets were used for training and the rest one for validation. A complete 10-fold cross-validation of the networks consisted of 10 such training cycles where each subset was utilized for validation purposes.

4. Results and Discussion

The neural network implementation, training, and testing were done in TensorFlow 2.4 and Python 3.8, which were installed and run on MacOS Big Sur with a 2.7GHz Dual-Core Intel Core i5 CPU. For PR-EOS modeling, non-zero binary interaction parameters (k_{ij}) were used. A k_{ij} of 0.1597 [6] for the binary mixture of C_{10}/N_2 and 0.1561 [17] for C_{12}/N_2 were used.

4.1 Unified Data-Driven Model using Interpolation (DD-Int)

In this section, the performance of the unified binary composition model trained using the interpolated dataset is discussed. The shape of the VLE curves for the binary mixtures of C_{10}/N_2 and C_{12}/N_2 change drastically as the temperature rises. Low temperatures are characterized by linear and steep slopes, indicating very high critical pressures for the concerned isotherm. On the other hand, at high temperatures, the liquid and vapor limbs of VLE curve towards each other in an apparent attempt to form a closed loop at low pressures. This also indicates that at higher temperatures, the mixture critical pressure will be lower. Given the change in the VLE behavior as a function of temperature, a data-driven model found it hard to exhibit good performance across all temperatures if it was trained on an equal number of points. As a result, the DD-Int model was trained asymmetrically, with the interpolation dataset having 2000 points for the low-temperature range and 3000 points for higher isotherms (≥ 503 K). Figures 4 and 5 show the VLE data on a pressure–composition plot for the binary mixtures of C_{10}/N_2 and C_{12}/N_2, respectively. The performance of the DD-Int model was gauged against the experimental data and PR-EOS modeled VLE data. From the VLE of both the n-alkane/nitrogen binary mixtures, it can be seen that for a fixed temperature, the solubility of nitrogen increases in the n-alkane rich liquid phase with the increase of pressure. For a fixed pressure, the solubility of nitrogen in the n-alkane rich liquid phase is also found to be directly proportional to the mixture temperature [6,17]. For isotherms above 463 K, the PR-EOS model deviated from the experimental data points at higher pressures. The DD-Int model, on the other hand, was able to capture the change in curvature of the VLE curves at higher pressures for both binary mixtures. For the 563.1 K isotherm of C_{10}/N_2 in Fig. 4, the DD-Int model predictions were closer to the PR-EOS modeled data than to the experimental data but still exhibited a change of curvature in the vapor arm of the curve at higher pressures, which was not captured by the EOS model. For the C_{12}/N_2 mixture, the DD-Int model showed good agreement with experimental trends across all isotherms and pressure ranges.

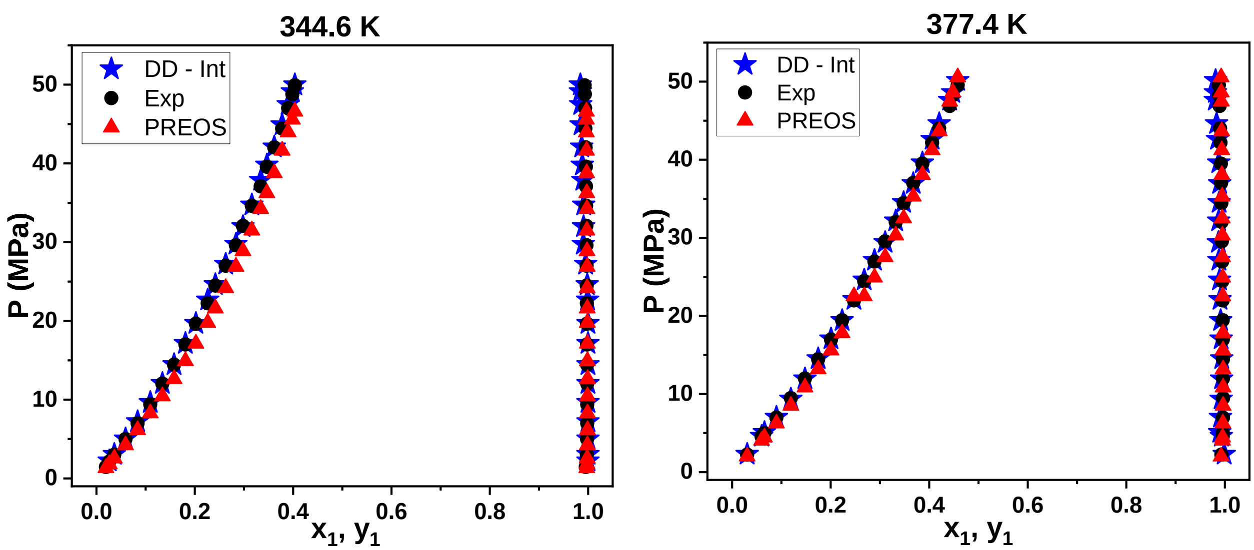

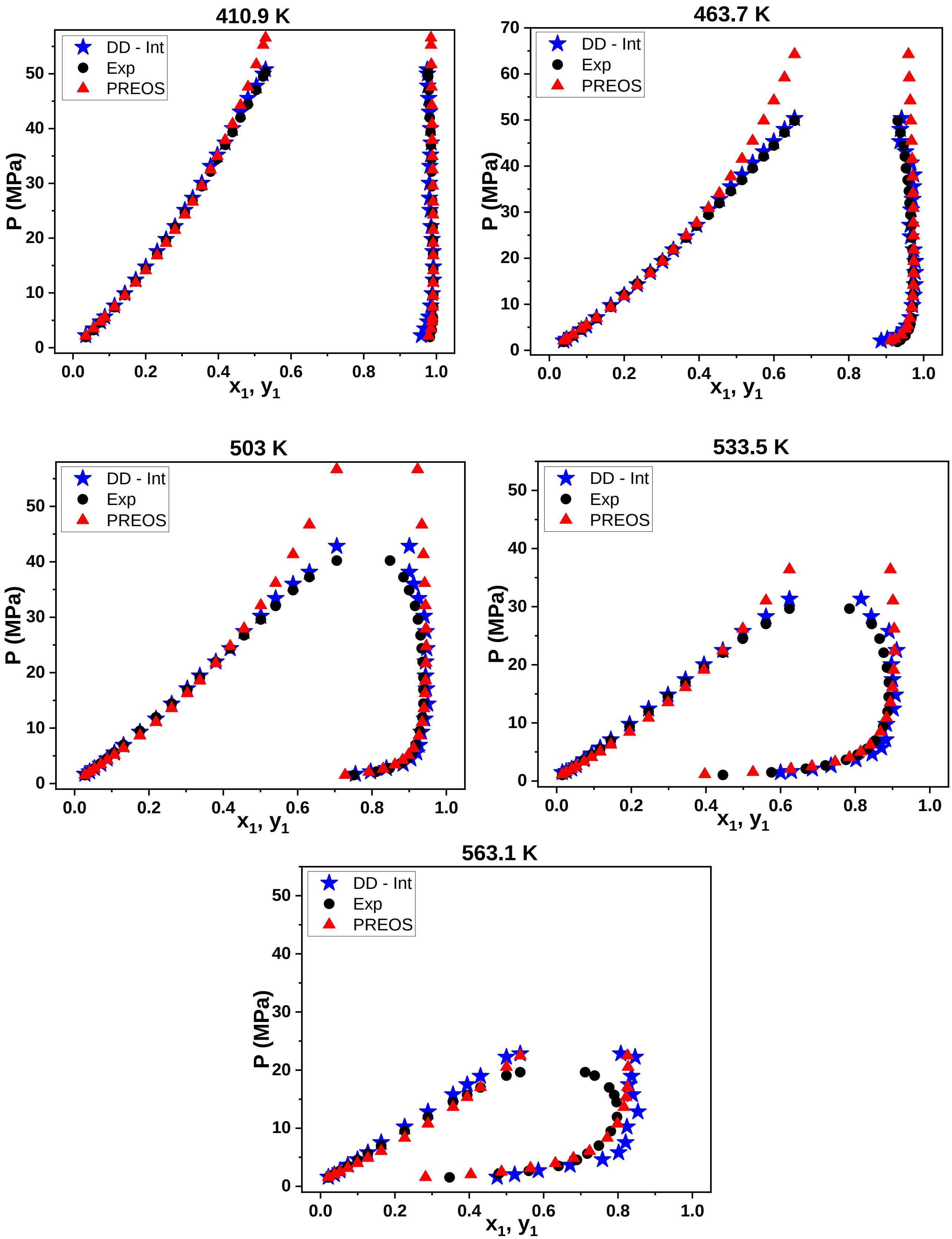
410.9 K
463.7 K
503 K
533.5 K
563.1 K
DD - Int
Exp
PREOS
P (MPa)
x1, y1

Fig 4. Comparison of VLE for the binary mixture of C_{10}/N_2 using: (a) DD-Int model (blue star), (b) Experiment data [6] (black circle), and (c) Peng-Robinson EOS (red triangle)

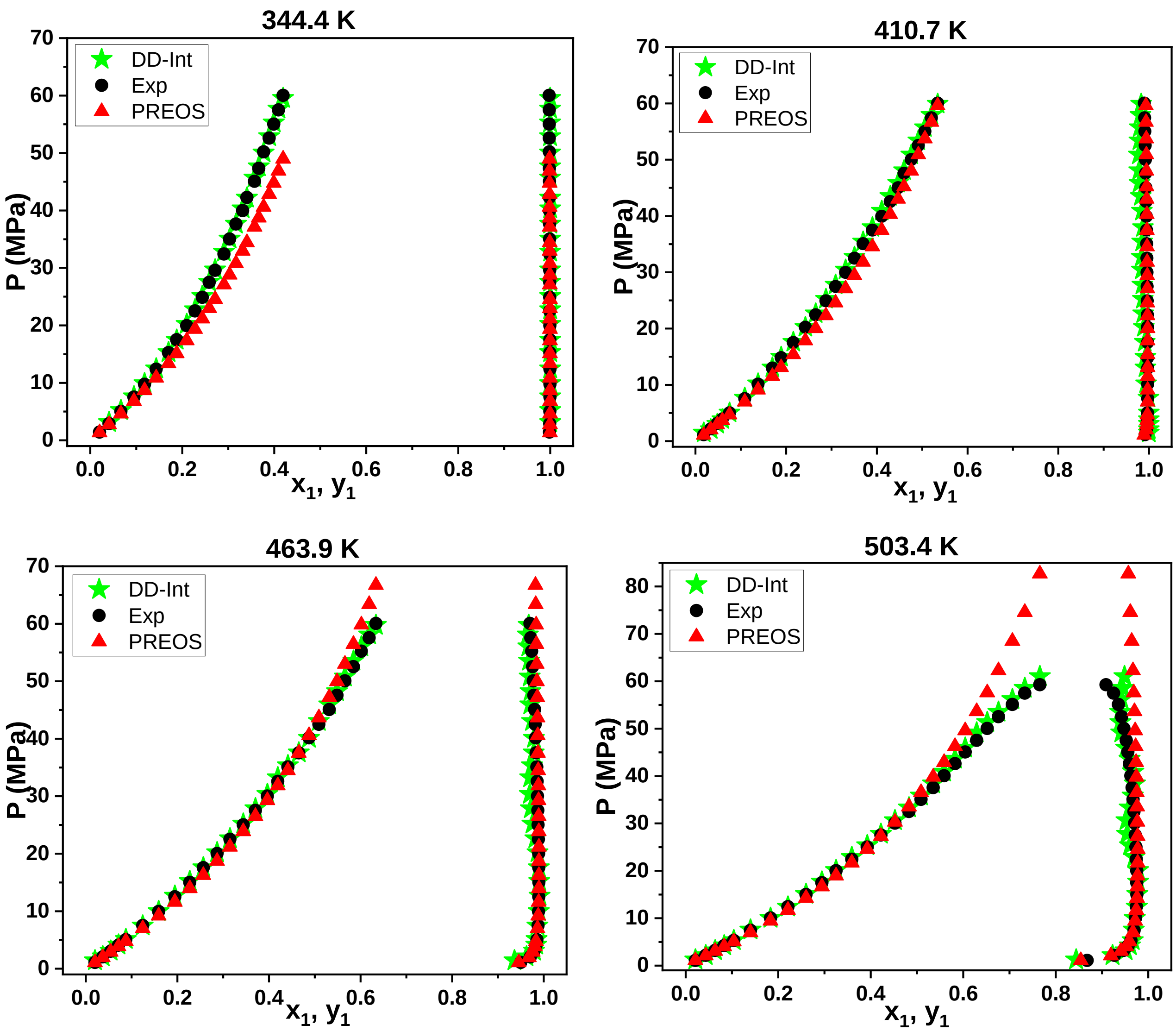

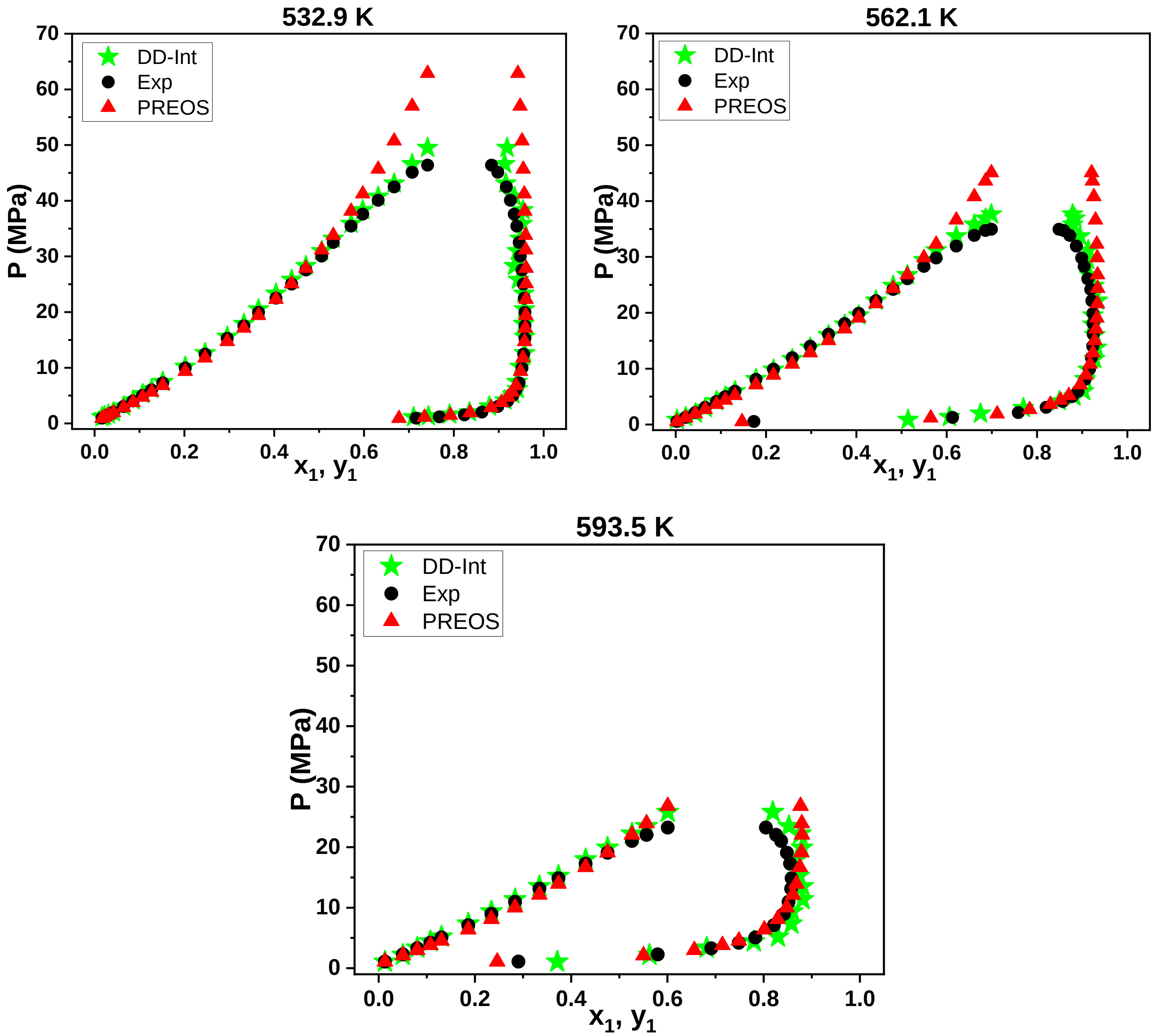

Fig 5. Comparison of VLE for the binary mixture of C_{12}/N_2 using: (a) DD-Int model (green star), (b) Experiment data [17] (black circle), and (c) Peng-Robinson EOS (red triangle)

Fig. 6 shows the mean value of the absolute percentage errors in pressure estimation as a function of temperature, for the EOS and DD-Int model. For both mixtures, it can be seen that the machine learning-based model had a much lower error as compared to the PR-EOS model. For the binary mixture of C_{10}/N_2, using the DD-Int model, the errors in pressure estimation were less than 3.4%, except for the 563.1 K, where the mean error jumped to ~7%, but still lower than the EOS model error. The error in estimating the vapor phase composition was also less than 3%, with the exception of ~7.5% for the 563.1 K isotherm. DD-Int modeled VLE for the binary system of C_{12}/N_2 had pressure errors in the range of [0.7 – 3.8] %, which was considerably lower compared to the error from the PR-EOS model. The pressure error from the DD-Int model exhibited a gradual increase in magnitude with the rise of temperature. The C_{12}/N_2 vapor phase composition predicted using the DD-Int model had errors in the range of [0.1 – 3.2] %, as opposed to [5 - 15] % from the PR-EOS model.

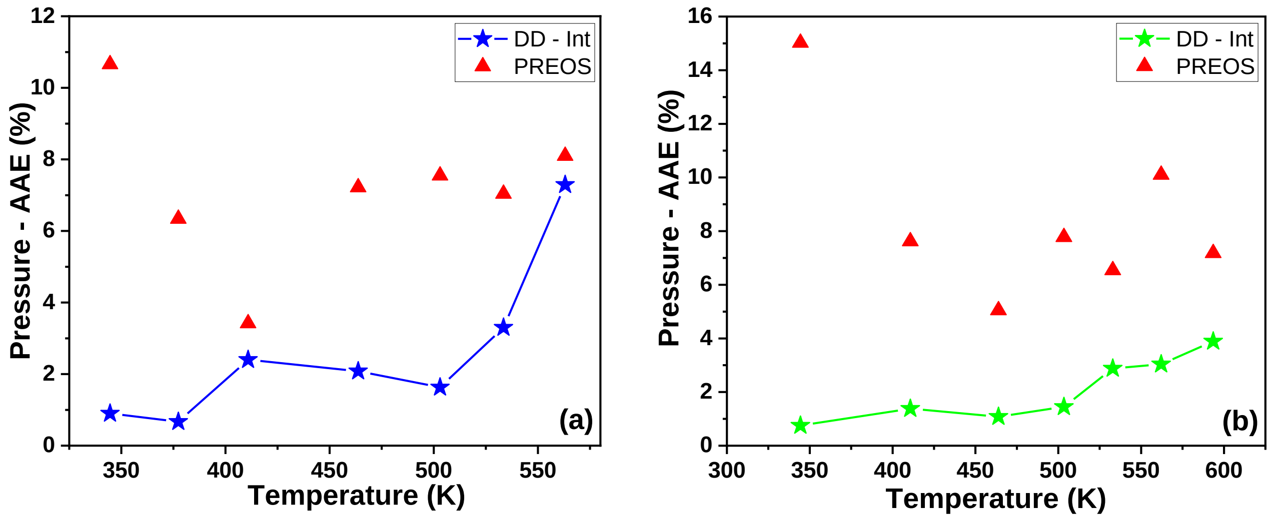

Fig 6. Model performance in estimating mixture equilibrium pressure: Data-driven interpolation model (DD-Int) vs PR-EOS for the binary mixtures of (a) C_{10}/N_2 and (b) C_{12}/N_2

4.2 Models based on Individual Isotherm Training

4.2.1 Unified Data-Driven Model using Individual Temperature Trained Models (DD-Ind-T)

In this section, the unified data-driven model (DD-Ind-T) was trained using the individually trained temperature models. The individual models were trained using the limited experimental data set available. The average model performance metric for each of the individual isotherm models is given in Table 2.

Table 2: R^2 and MSE for the individual temperature models

Mixture	Temperature [K]	MSE	R^2
C_{10}/N_2	344.6	0.0536	0.9996
	377.4	0.0649	0.9997
	410.9	0.0290	0.9992
	463.7	0.0364	0.9998

	503	0.1349	0.9944
	533.5	0.0378	0.9995
	563.1	0.0893	0.9950
	344.4	1.2012	0.9924
	410.7	0.6130	0.9970
	463.9	1.0047	0.9661
C_{12}/N_2	503.4	0.5138	0.9928
	532.9	0.4469	0.9969
	562.1	0.0731	0.9987
	593.5	0.0491	0.9680

The individually trained models were used to generate 2000 data points for each temperature by taking randomly sampled liquid phase mixture compositions (x_1 and x_2). This newly generated dataset was then used to train the new unified data-driven model (DD-Ind-T). Figures 7 and 8 show the DD-Ind-T modeled VLE data on a pressure–composition plot for both the binary mixtures and their comparison with experimental data and PR-EOS model. Similar to the DD-Int model, the DD-Ind-T model was also capable of capturing the correct trend of increase in nitrogen solubility in the n-alkane rich liquid phase, with the increase of pressure and temperature [6,17].

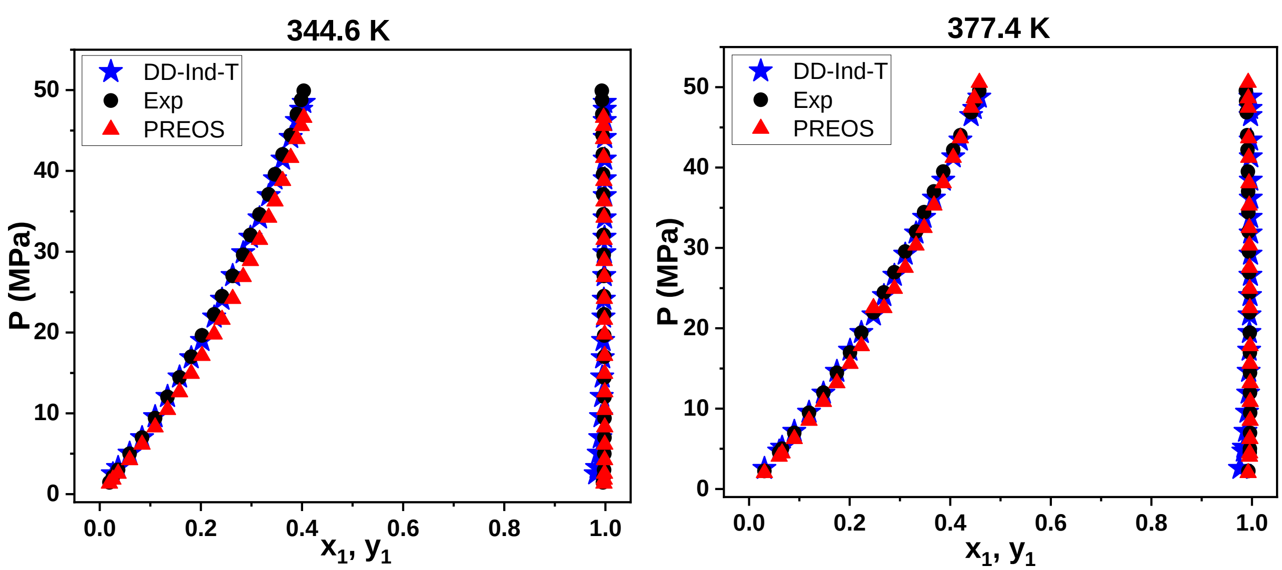

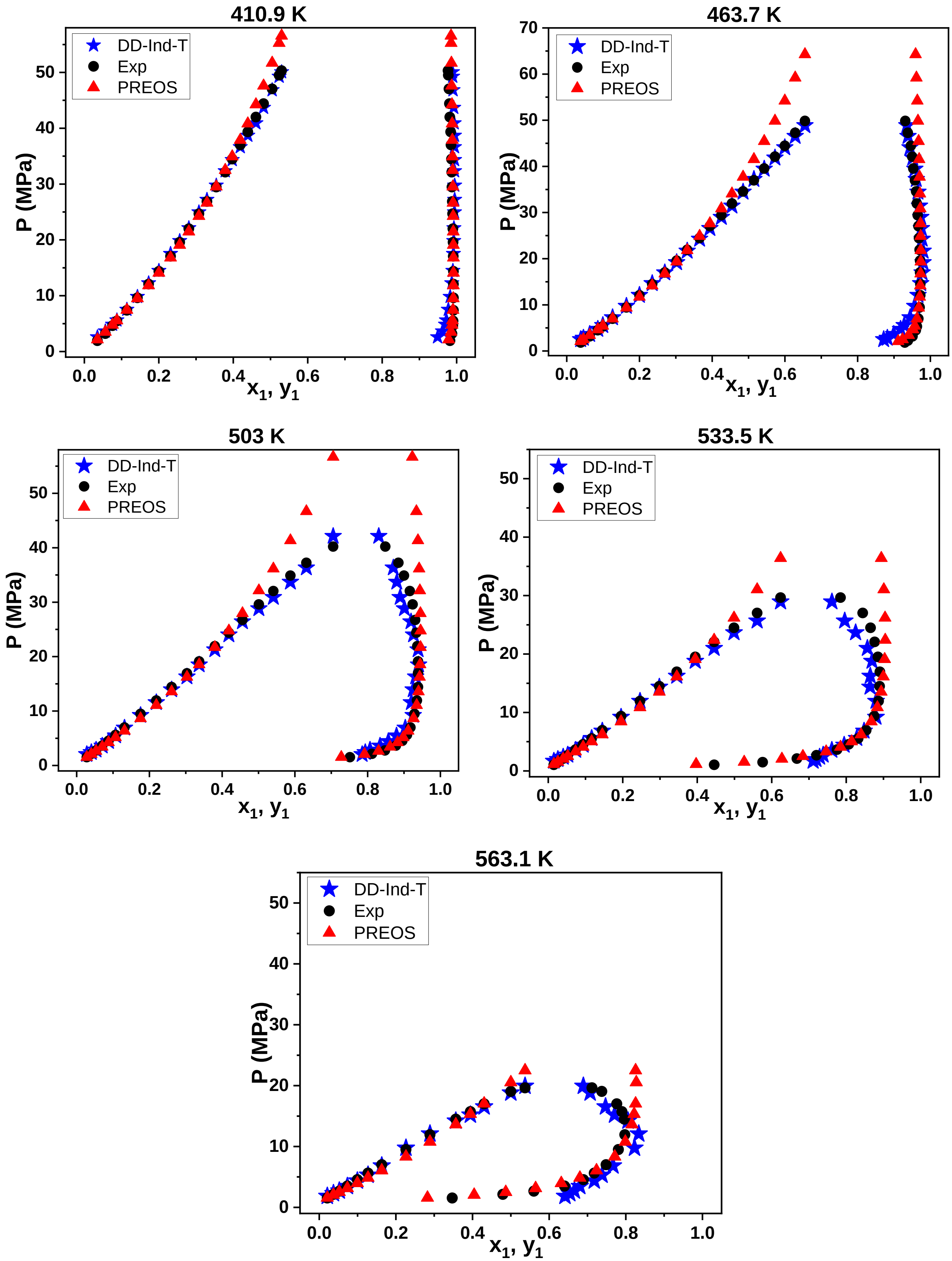
410.9 K
463.7 K
503 K
533.5 K
563.1 K
DD-Ind-T
Exp
PREOS
P (MPa)
x1, y1

Fig 7. Comparison of VLE for the binary mixture of C_{10}/N_2 using: (a) DD-Ind-T model (blue star), (b) Experiment data [6] (black circle), and (c) Peng-Robinson EOS (red triangle)

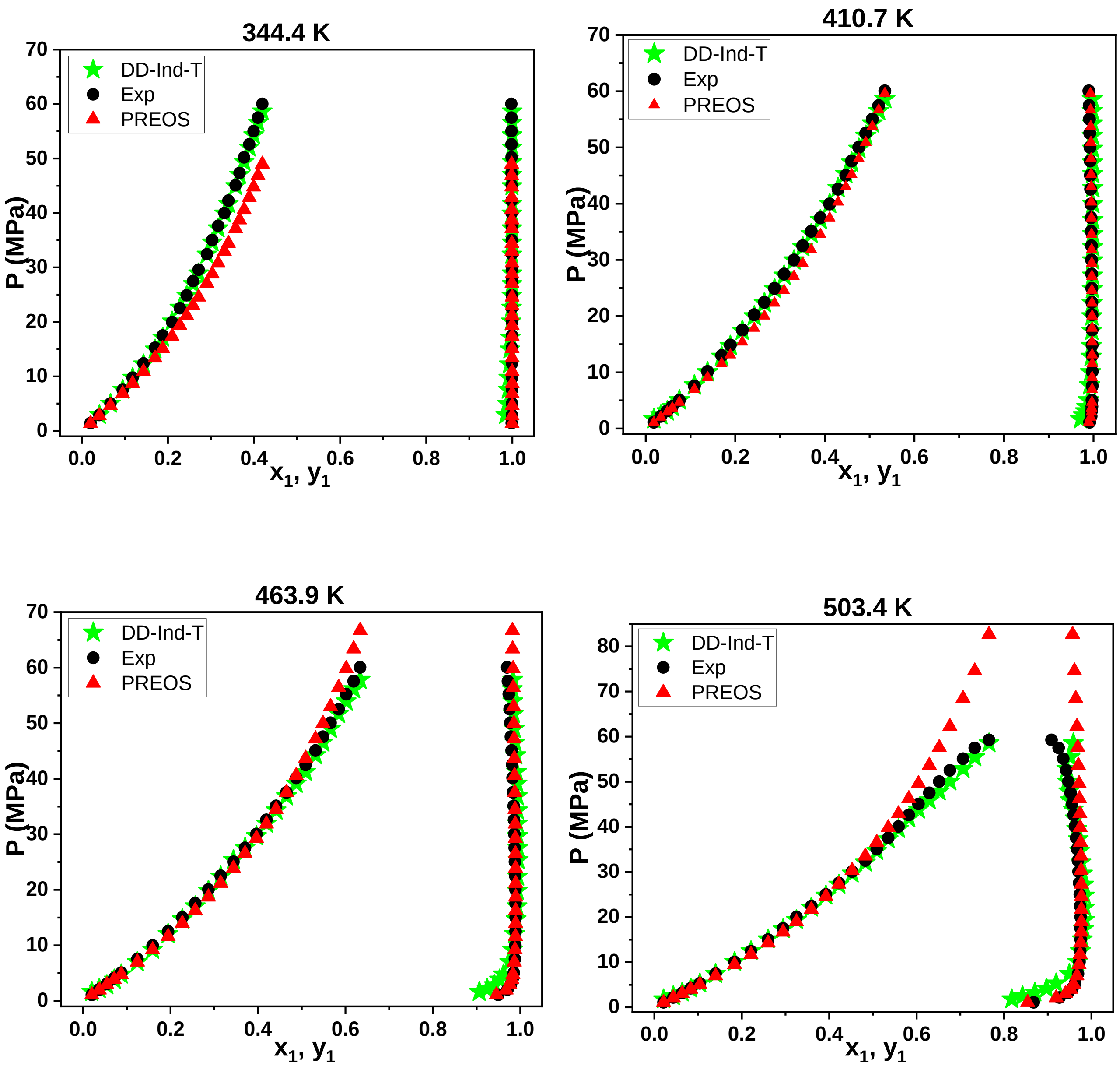

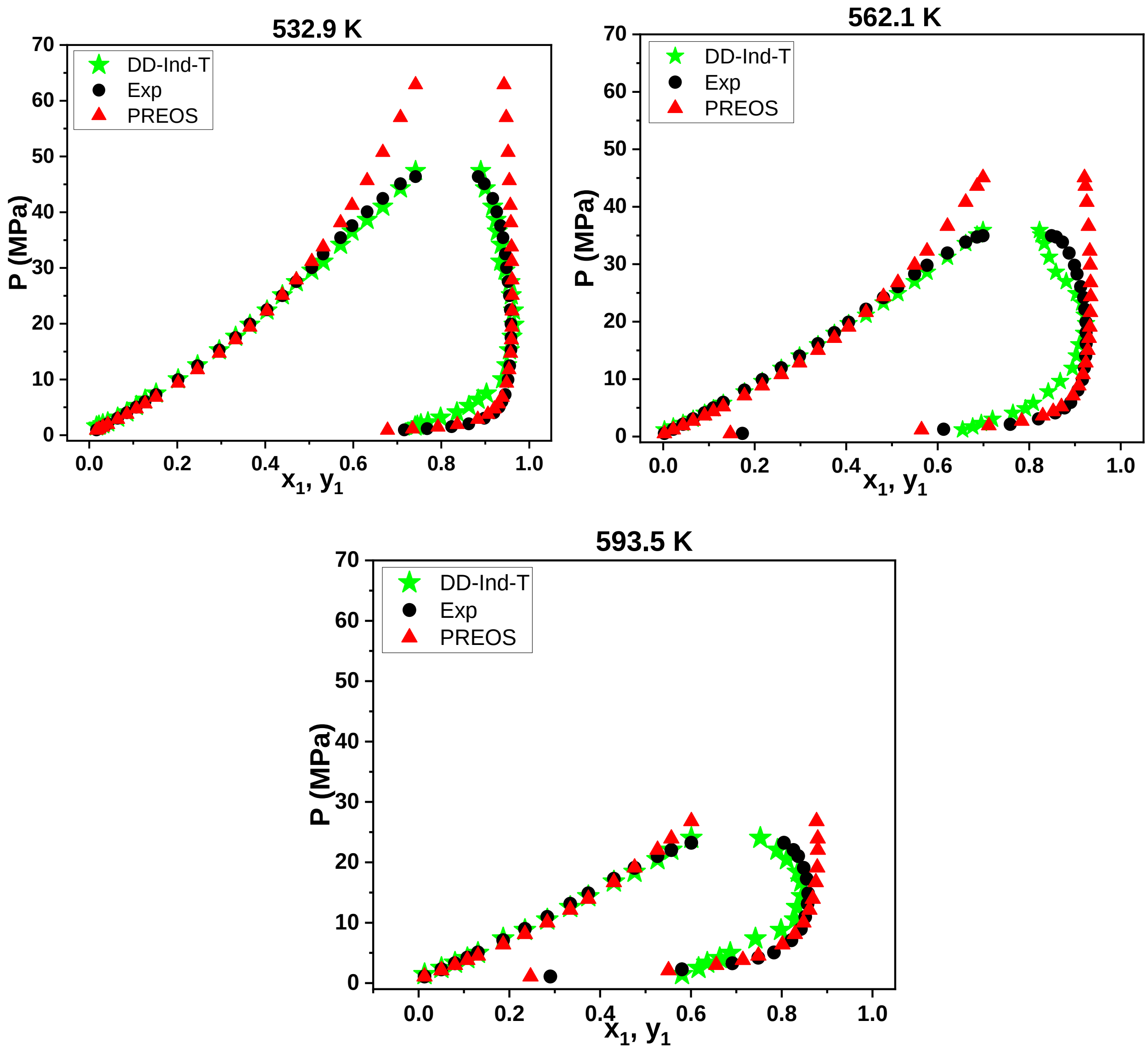

Fig 8. Comparison of VLE for the binary mixture of C_{12}/N_2 using: (a) DD-Ind-T model (green star), (b) Experiment data [17] (black circle), and (c) Peng-Robinson EOS (red triangle)

The DD-Ind-T model showed improvement over the DD-Int model in being able to track the changing curvatures of the vapor phase curve at high pressures, even for the high temperature (563.1 K) isotherm of the C_{10}/N_2 system. A comparison of the average absolute error plots in predicting pressure, using the DD-Ind-T and PR-EOS models, for the binary mixtures of C_{10}/N_2 and C_{12}/N_2 is shown in Fig. 9. For the C_{10}/N_2 mixture, the pressure errors were in the range of [1.5 – 5.2] %, whereas the PR-EOS model had errors of the order of [3.4 – 10.6] %. The DD-Ind-T model also exhibited a slight increase in the mean error magnitudes with the increase of temperature. The pressure and vapor composition errors, for C_{12}/N_2, using the DD-Ind-T model, were in the ranges of [1.3 – 4.2] % and [0.5 – 5.3] % respectively. Using the PREOS model resulted in higher errors for the pressure of the order of [5 – 10.1] % for the C_{12}/N_2 binary system. However, the DD-Ind-T model found it hard to correctly estimate the vapor phase composition at extremely low pressures of 1 MPa for higher temperature isotherms (T ≥ 533 K).

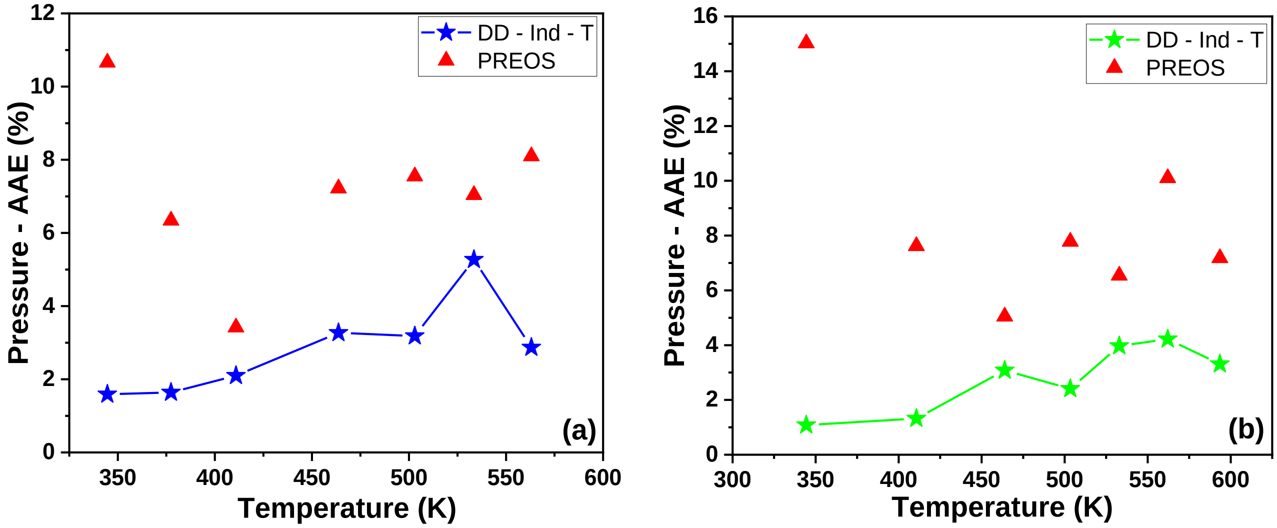

Fig 9. Model performance in estimating mixture equilibrium pressure: data-driven individual temperature trained model (DD-Ind-T) vs PREOS for the binary mixtures of (a) C_{10}/N_2 and (b) C_{12}/N_2

4.2.2 Improved DD-Ind-T Model (DD-Ind-T-v2)

In this section, the DD-Ind-T model was improved by infusing more physics about a phase envelope into the model. The goal was to make the new model (DD-Ind-T-v2) aware of the critical locus of the Type-III binary systems (C_{10}/N_2 and C_{12}/N_2) under consideration. Finally using the newly trained model to generate the phase envelopes for a wide range of isotherms; the peak of the envelope in each case will correspond to the mixture critical pressure for that particular isotherm. Fig. 10 (a) and (b) show the critical locus line for the binary mixtures of C_{10}/N_2 and C_{12}/N_2 respectively. The data for the mixture critical points of C_{10}/N_2 were taken from the works of Garcia-Sanchez et al. [6] and M. Wirths [50]. Data for the mixture critical points of C_{12}/N_2 was taken from Garcia-Cordova et al. [17]. Type-III behavior of the mixtures is clear from the plots, with one end of the discontinuous critical locus line (starting from the heavier component, n-alkane) shooting up to very high-pressure values.

The other half of the discontinuous locus (not shown in the plot) would start at the lighter component (N_2) and end in a VLLE.

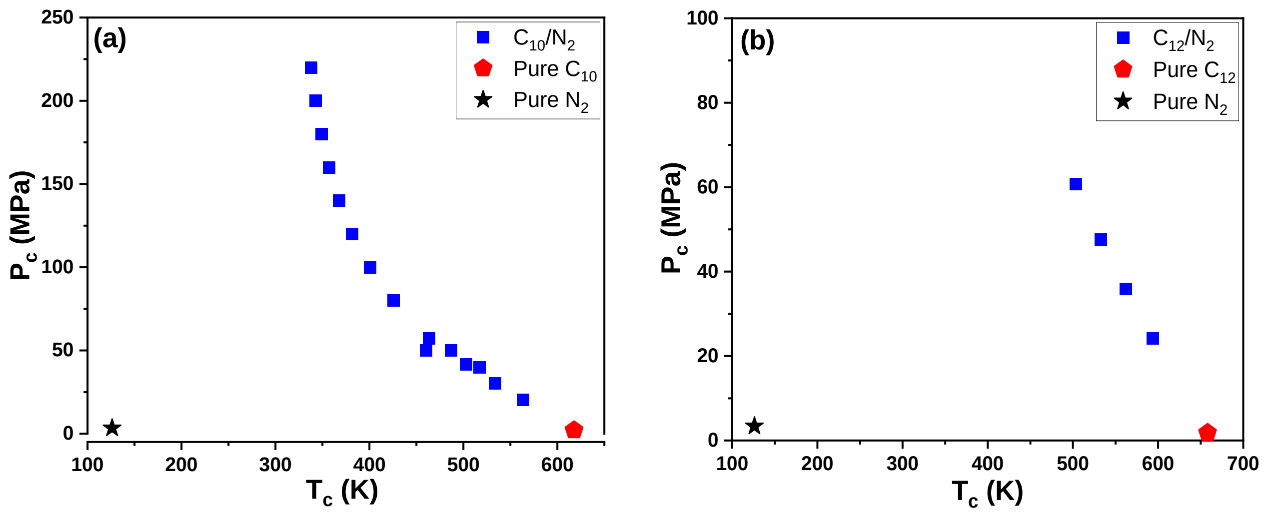

Fig 10. Mixture critical points for the binary system of (a) C_{10}/N_2 and (b) C_{12}/N_2, superimposed with pure component critical points

By fitting polynomials to the critical locus data available, we obtain empirical relations which can then be used in training the data-driven models. For the binary mixture of C_{10}/N_2, the proposed fitting is split into two temperature zones, with $T_c \geq 463.7\ K$ being modeled using a linear fit and $T_c < 463.7\ K$ being modeled using a quadratic fit.

For C_{10}/N_2:

$$P_c = \begin{cases} A_0 + A_1\, T_c, & if\ T_c \geq 463.7\ K \\ A_2 + A_3 T_c + A_4 T_c^2, & otherwise \end{cases} \tag{4.1}$$

where for the linear model, $A_0 = 229.12373 \pm 0.1669$ and $A_1 = -0.37204 \pm 3.24587 \times 10^{-4}$. And for the quadratic model, $A_2 = 1301.39707 \pm 124.8647$, $A_3 = -4.77202 \pm 0.57887$ and $A_4 = 0.00448 \pm 6.54863 \times 10^{-4}$.

Not much data is available on the critical locus for the binary of C_{12}/N_2. The data obtained from the works of Garcia-Cordova et al. [17] was fitted using a quadratic expression, as shown in equation 4.2.

For C_{12}/N_2:

$$P_c = B_0 + B_1 T_c + B_2 T_c^2 \tag{4.2}$$

where, $B_0 = 430.65881 \pm 14.38436$, $B_1 = -1.01457 \pm 0.05259$ and $B_2 = 5.55399 \times 10^{-4} \pm 0.05259$.

While training the new model (DD-Ind-T-v2), it was important to impose the mixture's pressure physical constraints, as learned from the critical locus, so that the neural network predictions do not exceed the physical limits even when the inputs are outside the range in the training set. To achieve this, the pressure value of each instance in the dataset during training was scaled to [0, 1] by dividing its corresponding pressure upper limit, as shown below.

$$\widetilde{P_i} = \frac{P}{P_i^M} \tag{4.3}$$

where, P_i is the current pressure value of instant i, P_i^M is the corresponding pressure upper limit obtained from equations 4.1 and 4.2, and $\widetilde{P_i}$ is the scaled value being used in the model training. While preserving the DD-Ind-T network architecture, a logistic activation function was placed at the pressure predicting node instead of the linear output. This activation function served the purpose of limiting the node output values to [0, 1]. Different from the sigmoid activation used in the other output node, there is a parameter α controlling the logistic growth rate of the function, as shown below.

$$\sigma(x) = \frac{1}{1 + e^{-\alpha x}} \tag{4.4}$$

where x is the node input. A small α leads to a slow growth rate of the function, allowing a wider range of x until function value saturation. The choice of α in this work is 0.01. In inference time, the model outputs scaled pressure for every new data point. The final predicted pressure value would be obtained by multiplying the model scaled pressure output with its corresponding pressure upper limit.

Figures 11 and 12 show the performance of the new DD-Ind-T-v2 model in estimating the phase envelope for the binary systems of C_{10}/N_2 and C_{12}/N_2 respectively. The results are compared with the experimental VLE data points from the works of Garcia-Sanchez et al. [6] and Garcia-Cordova et al. [17]. The new model performs really well, across a wide range of temperatures, in estimating the vapor phase composition and equilibrium pressure for the binary systems under consideration and the result agrees well with the experimental data as shown in Figs. 11 and 12. Moreover, the DD-Ind-T-v2 model is successfully estimating a smooth and continuous phase envelope having VLE points beyond the range of the existing experimental data set used to train the model. The peak of each phase envelope is representative of the mixture critical pressure of that particular isotherm. For the binary mixture of C_{12}/N_2 only four isotherms (503.4 K - 593.5 K) are shown in Fig. 12 since the model was trained on critical locus data for the same mixture in that same temperature range. The DD-Ind-T-v2 model can definitely produce phase envelopes for C_{12}/N_2 and for a temperature isotherm outside the mentioned range, but it will be hard to validate the critical pressure of that envelope due to the lack of experimental data.

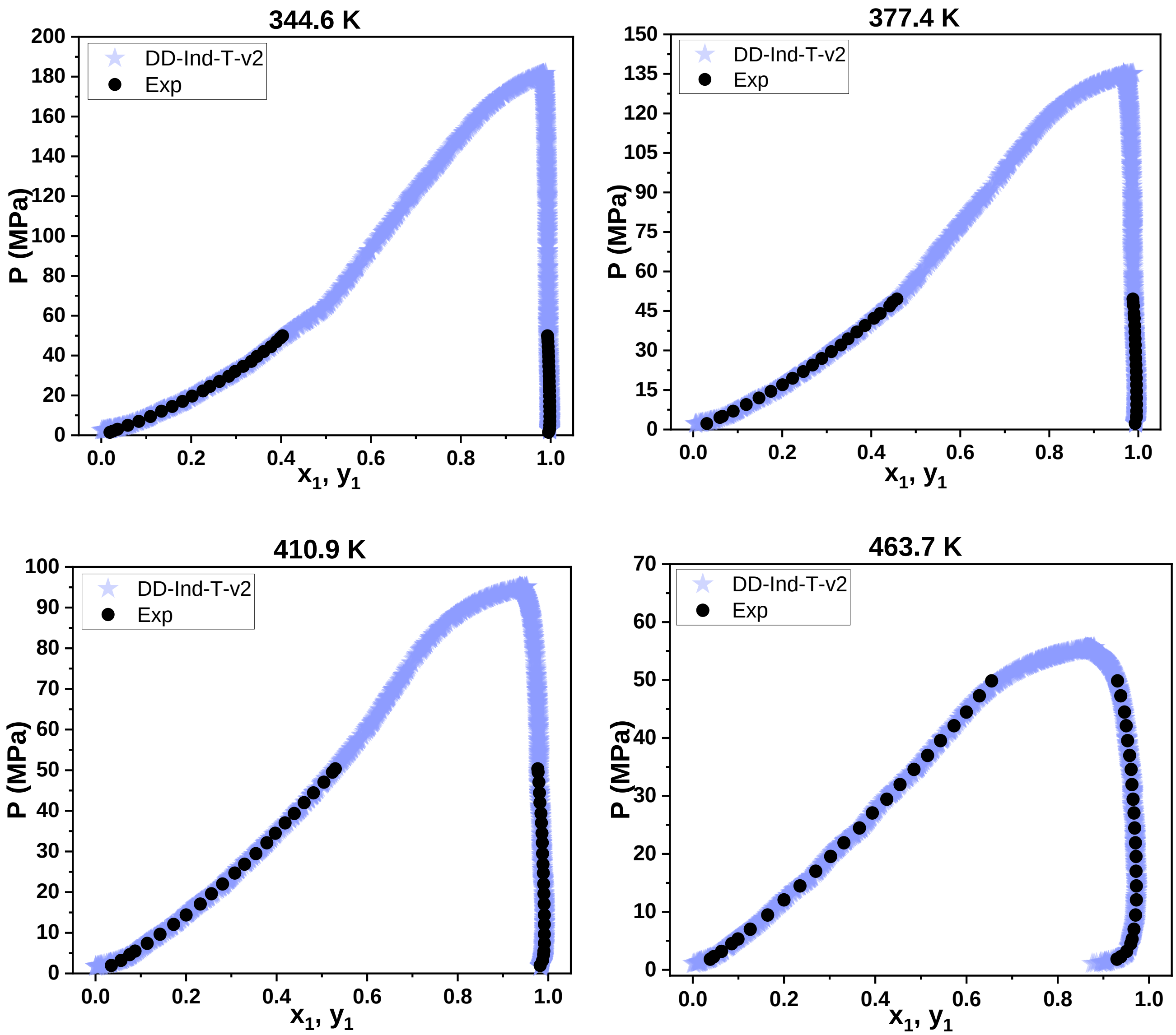

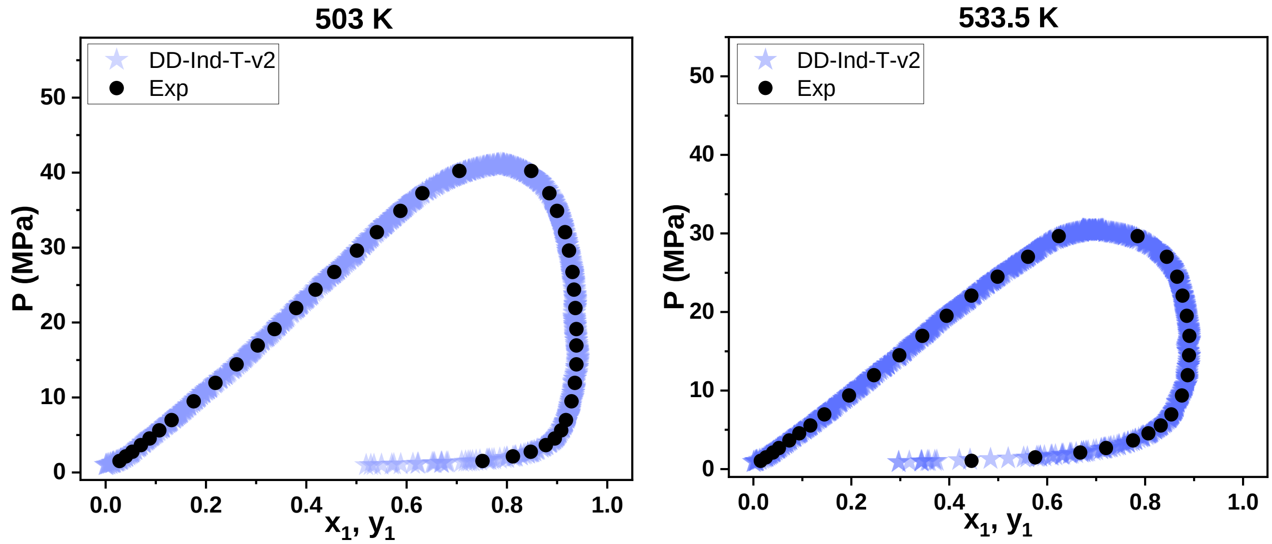

Fig 11. Comparison of phase envelop for the binary mixture of C_{10}/N_2 using: (a) DD-Ind-T-v2 model (blue star) and (b) Experiment VLE data [6] (black circle).

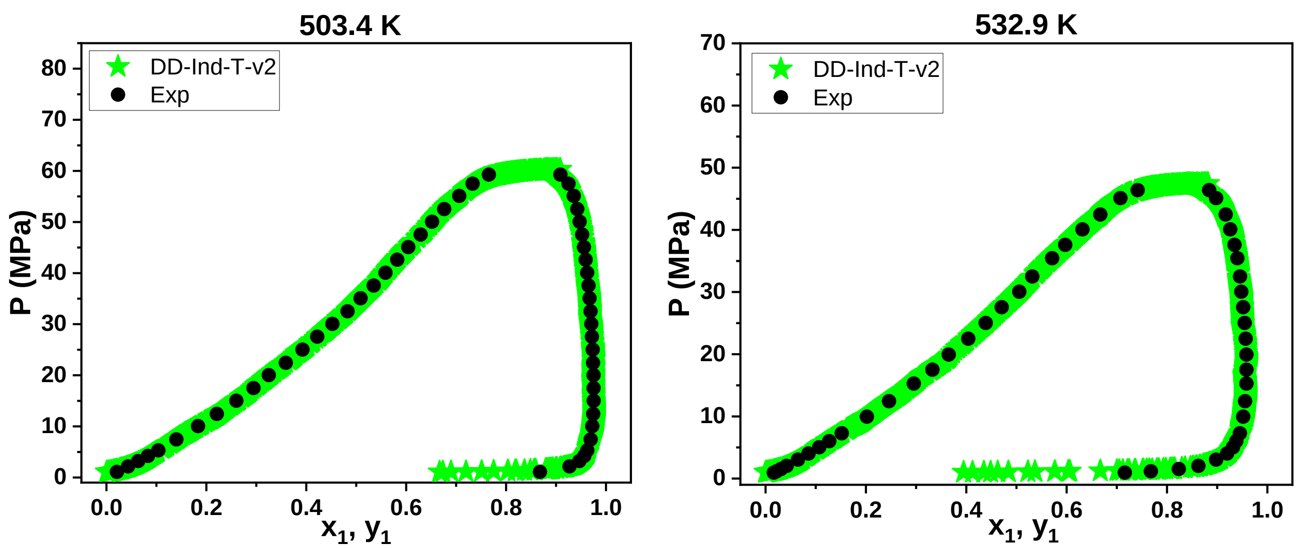

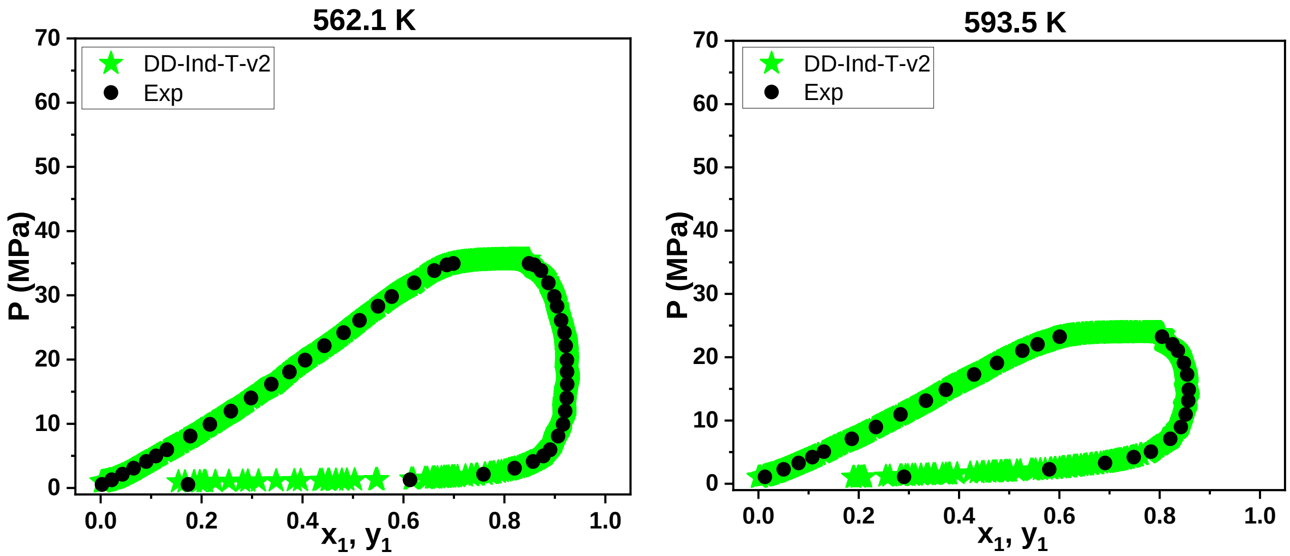

Fig 12. Comparison of phase envelope for the binary mixture of C_{12}/N_2 using: (a) DD-Ind-T-v2 model (green star) and (b) Experiment VLE data [17] (black circle).

Figure 13 shows the phase envelope estimated using the DD-Ind-T-v2 model for the binary mixture of C_{10}/N_2 at 563.1 K. This is the only isotherm in which the new model exhibited slight deviations from the experimental VLE data points. The peak of the phase envelope is still consistent with the critical pressure (~20 MPa) of this binary mixture at the critical temperature of 563.1 K. This limitation or discrepancy of the model can be explained by referring back to Table 1, which summarizes the available experimental data points used in this study. The isotherm of 563.1 K has only 14 data points available. Availability of more experimental data points can considerably improve the performance at this isotherm, as already exhibited for other isotherms having more experimental data points to train the model on.

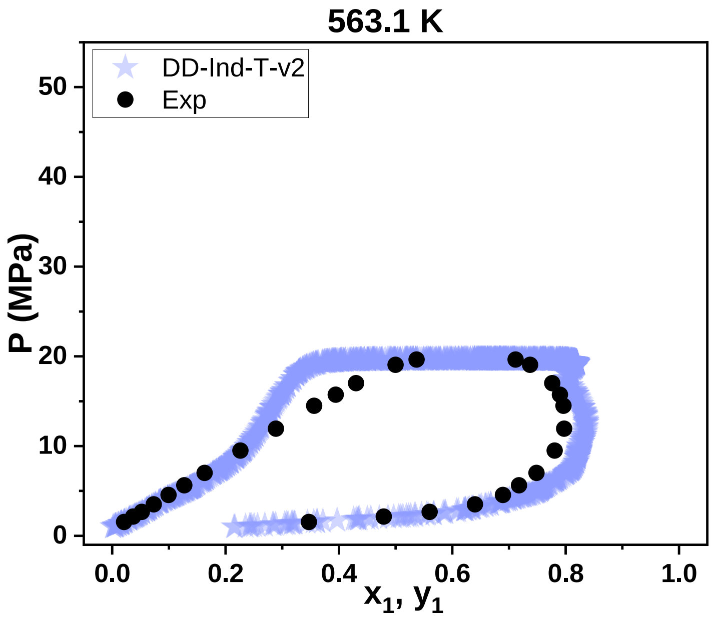

Fig 13. Phase envelop of C_{10}/N_2 at 563.1 K using: (a) DD-Ind-T-v2 model (blue star) and (b) Experiment VLE data [6] (black circle).

4.3 Model extension to ternary mixture phase equilibrium

In this section, the application of the proposed network architecture was extended to estimate the vapor-liquid-equilibrium of a ternary system of n-alkanes and nitrogen. The three-component system comprises methane (CH_4, component-1), n-decane (C_{10}, component-2), and nitrogen (N_2, component-3). Methane may also be referred to as C_1 in the following sections. A summary of the data set size used for the ternary mixture is presented in Table 3.

Table 3: Summary of VLE Experimental Data Set for $C_{10}/N_2/C_1$

Mixture	Temperature [K]	No. of points	Source
$C_1/C_{10}/N_2$	310.9	44	Azarnoosh et al. [51]
	344.3	41	
	377.6	45	
	410.9	44	

The neural network for the ternary system adopted the same architecture and loss function as the composition-specific models. A few layer-level modifications were made to fit the data of the ternary system. Firstly, the network input layer had 4 nodes, taking temperature, x_1, x_2, and x_3 (liquid phase composition of the three-component system) as inputs, respectively. Secondly, the output layer was set to have 3 nodes, predicting equilibrium pressure, y_1, and y_2 (vapor phase composition), respectively. The mole fractions in the liquid (x_i) and vapor (y_i) phase should individually sum up to one respectively. Lastly, due to the more significant scale difference in target values, and to ensure effective optimization in training, the target values were scaled to [0, 1], and inversely transformed back to the original scale during evaluation. As a result, the activation function limiting the range of vapor composition was changed to rectified linear units, which were used in all hidden layers. The strength of the experimental data set of the ternary system for each isotherm was almost twice as large as compared to the binary systems. Thus, they were directly used for model training. A 90-10 split was done for each isotherm data set, using 90% of the data for training and the remaining 10% as the test data set. The average model training metric in predicting the equilibrium pressure and vapor phase composition (y_1 and y_2), for each of the individual isotherms, is given in Table 4.

Table 4: New model performance (R^2) in training for ternary system

Mixture	Temperature [K]	Pressure - R^2	y_1 - R^2	y_2 - R^2
$C_1/C_{10}/N_2$	310.9	0.9984	0.9964	0.9358
	344.3	0.9993	0.9996	0.9900
	377.6	0.9995	0.9983	0.9866
	410.9	0.9999	0.9986	0.9968

Fig. 14 shows parity plots comparing various parameters of VLE for the ternary system of methane/n-decane/nitrogen. Fig. 14(a) shows the estimated and experimental equilibrium pressure for each other the four isotherms in the test data set. The pressure estimation on the test set has an average R^2 of 0.9957. Figs. 14(b)-(d) shows the experimental and estimated vapor phase mole fractions of methane, nitrogen, and n-decane respectively. The average performance in estimating the vapor phase mole fractions in terms of R^2 is 0.9900 (methane, y_1), 0.9898 (nitrogen, y_3), and 0.9350 (n-decane, y_2).

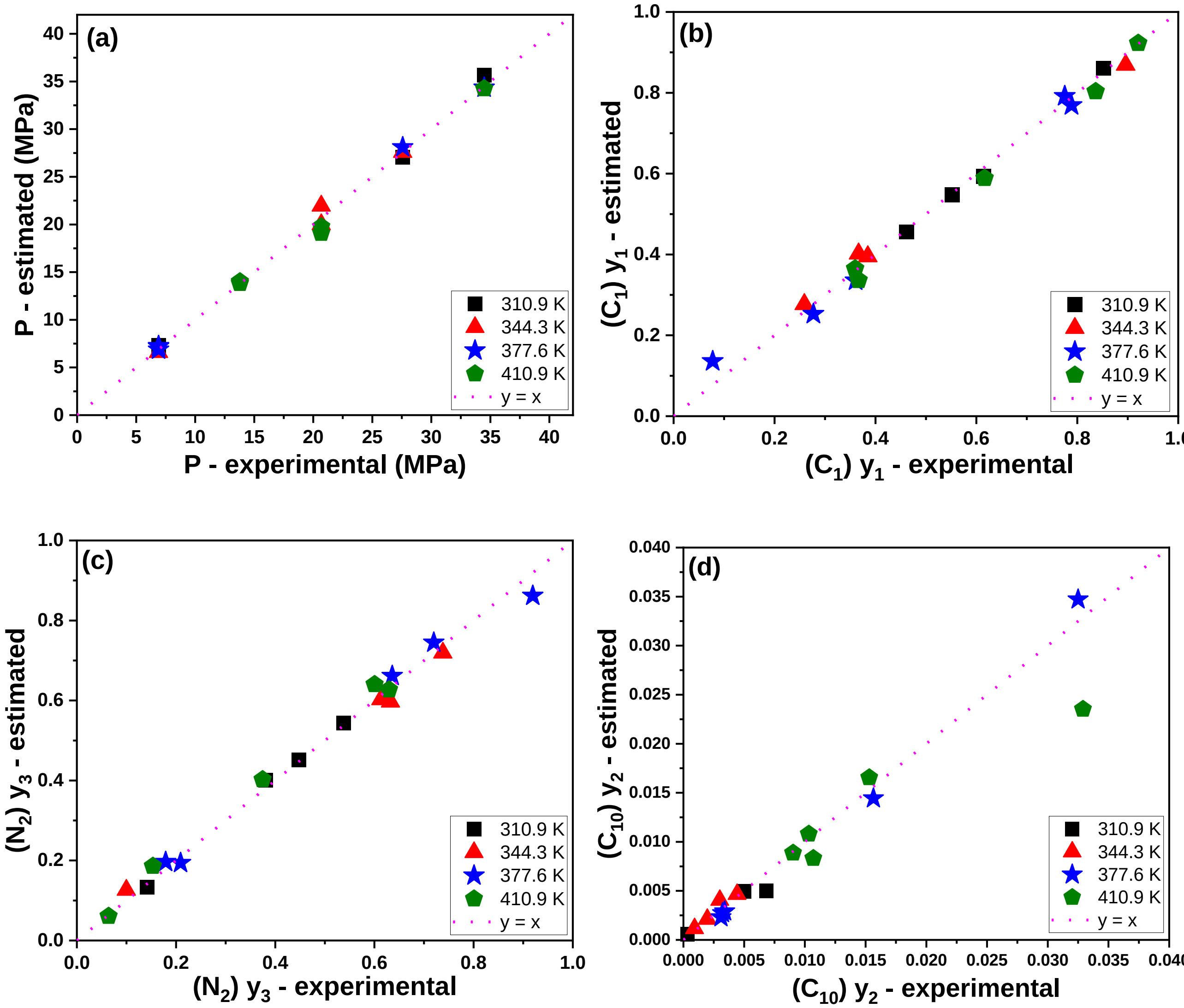

Fig 14. Comparison of estimated equilibrium parameters for the ternary system of $C_1/C_{10}/N_2$: data-driven model vs experimental data [51]. (a) equilibrium pressure, (b) methane vapor phase composition, (c) nitrogen vapor phase composition, and (d) n-decane vapor phase composition.

The R^2 values from both the training set (Table 4) and test data set (Fig. 14) reflect that the model has been able to capture the features of the ternary system phase equilibrium quite accurately. In the case of estimating vapor mole fraction of C_{10}, the spread of the experimental values ssis of the order of $10^{-3} – 10^{-2}$, and hence even small deviations from the actual value can lower the R^2 considerably.

5. Conclusions

Data-driven learning-based unified models were proposed in this study to predict the vapor-liquid equilibrium of binary and ternary mixtures involving long-chain n-alkanes and nitrogen. One of the models (DD-Int) was trained based on the interpolated dataset generated using the experimental data. The second model (DD-Ind-T) was trained based on the data generated from individually trained temperature-based sub-models. VLE of the two binary mixtures was also modeled using the Peng-Robinson equation of state and compared against that of the machine learning-based models.

Both machine learning-based models were able to predict the equilibrium pressure of the binary mixtures with considerably less error as compared to the PR-EOS model. The improvement in accuracy came with the added advantage of being completely independent of a binary interaction parameter. This parameter plays a crucial role in the mixing rules used in the EOS-based VLE model but is not readily available due to the lack of properties/experimental data of the pure components, which are not readily available.

The two machine learning-based models exhibited an increase in error in estimating equilibrium pressure, as the temperature of the mixture increases. The PR-EOS model failed to trace the curvature of the vapor phase exhibited at high pressures, close to the mixture critical point, at large temperatures. Both DD-Int and DD-Ind-T models, on the other hand, were successful in tracing the change of slopes of the vapor phase curves at higher pressures and temperatures. The DD-Ind-T model however was not able to correctly predict the vapor phase composition at low pressures (~ 1 MPa) and high temperatures. An upgrade to the DD-Ind-T model (DD-Ind-T-v2), which was trained using the critical locus data of the two binary mixtures, was able to estimate the complete phase envelope across a wide range of isotherms. In doing so, the model was able to estimate VLE points in the vicinity of the mixture critical point, which was beyond the range of the experimental data set on which the model was trained, and also something which a PR-EOS model fails to estimate. Moreover, estimating the full phase envelope also aids in exhibiting the mixture critical pressure of the binary system for that particular isotherm. In an attempt to demonstrate the flexible and versatile nature of the proposed model, the same network architecture was applied to a three-component (methane/n-decane/nitrogen) system. The model was able to learn the features of the ternary system VLE and estimate the equilibrium pressure and vapor phase mole fractions will good accuracy.

The availability of experimental data on VLE of long-chained n-alkane and nitrogen mixtures at high pressures and temperatures was few and far between. The models proposed in this study were shown to be robust, even though very limited experimental data points were used (each isotherm having 15–27 data points for the binary systems). The results suggested that the DD-Int and DD-Ind-T models could be used as a non-iterative, computationally efficient tool to predict VLE data for hydrocarbon mixtures such as C_{10}/N_2 and C_{12}/N_2 mixtures at high pressures and temperatures, even close to mixture critical point. In addition, the results also suggested that such models can be used in the future to help determine parameters in EOS models such as the temperature-dependent binary interaction parameter for given mixtures.

Acknowledgments

GL and YS gratefully acknowledge the support from the National Science Foundation (DMS-1555072, DMS-2053746, and DMS-2134209), and Brookhaven National Laboratory Subcontract 382247, and U.S. Department of Energy (DOE) Office of Science Advanced Scientific Computing Research program DE-SC0021142.

References

[1] R.D. Reitz, Modeling Atomization Processes in High-Pressure Vaporizing Sprays, Atomization and Spray Technology. 3 (1987) 309–337.

[2] R.D. Reitz, J.C. Beale, Modeling Spray Atomization With The Kelvin-Helmholtz/Rayleigh-Taylor Hybrid Model, Atomization and Sprays. 9 (1999) 623–650. https://doi.org/10.1615/atomizspr.v9.i6.40.

[3] L. Qiu, R.D. Reitz, An Investigation of Thermodynamic States During High-Pressure Fuel Injection using Equilibrium Thermodynamics, International Journal of Multiphase Flow. 72 (2015) 24–38. https://doi.org/10.1016/j.ijmultiphaseflow.2015.01.011.

[4] L. Qiao, S. Jain, G. Mo, Molecular Simulations to Research Supercritical Fuel Properties, in: J. Bellan (Ed.), High Pressure Flows for Propulsion Applications, AIAA Progr, 2020.

[5] W.L. Luyben, Distillation Design and Control Using Aspen™ Simulation, 2nd ed., John Wiley & Sons, Inc., Hoboken, New Jersey, 2013. https://doi.org/10.1002/9781118510193.

[6] F. García-Sánchez, G. Eliosa-Jiménez, G. Silva-Oliver, B.E. García-Flores, Vapor-liquid equilibrium data for the nitrogen + n-decane system from (344 to 563) K and at pressures up to 50 MPa, Journal of Chemical and Engineering Data. 54 (2009) 1560–1568. https://doi.org/10.1021/je800881t.

[7] P.H. van Konynenburg, R.L. Scott, Critical Lines and Phase Eqilibria in Binary van der Waals Mixtures, Philosophical Transactions of The Royal Society of London: A Mathematical and Physical Sciences. 298 (1980) 495–540.

[8] R. Privat, J.-N. Jaubert, F. Mutelet, Addition of the Nitrogen Group to the PPR78 Model (Predictive 1978, Peng Robinson EOS with Temperature-Dependent Kij Calculated through a Group Contribution Method), Industrial and Engineering Chemistry Research. 47 (2008) 2033–2048.

[9] R. Privat, J.N. Jaubert, F. Mutelet, Use of the PPR78 model to predict new equilibrium data of binary systems involving hydrocarbons and nitrogen. Comparison with other GCEOS, Industrial and Engineering Chemistry Research. 47 (2008) 7483–7489. https://doi.org/10.1021/ie800636h.

[10] A. Azarnoosh, J.J. Mcketta, Nitrogen-n-Decane System in the Two-Phase Region, Journal of Chemical and Engineering Data. 8 (1963) 494–496. https://doi.org/10.1021/je60019a005.

[11] F.M. Llave, T. Horng Chung, Vapor-Liquid Equilibria of Nitrogen-Hydrocarbon Systems at Elevated Pressures, Journal of Chemical and Engineering Data. 33 (1988) 123–128. https://doi.org/10.1021/je00052a019.

[12] J. Tong, W. Gao, R.L. Robinson, K.A.M. Gasem, Solubilities of nitrogen in heavy normal paraffins from 323 to 423 K at pressures to 18.0 MPa, Journal of Chemical and Engineering Data. 44 (1999) 784–787. https://doi.org/10.1021/je980279n.

[13] S.G. D'Avila, B.K. Kaul, J.M. Prausnitz, Solubilities of Heavy Hydrocarbons in Compressed Methane and Nitrogen, Journal of Chemical and Engineering Data. 21 (1976) 488–491. https://doi.org/10.1021/je60071a017.

[14] J.M. Prausnitz, P.R. Benson, Solubility of Liquids in Compressed Hydrogen, Nitrogen, and Carbon Dioxide, AIChE Journal. 5 (1959) 161–164.

[15] D.L. Pearce, C.J. Peters, J. de Swaan Arons, Measurement of the gas phase solubility of decane in nitrogen, Fluid Phase Equilibria. 89 (1993) 335–343. https://doi.org/10.1016/0378-3812(93)85092-Z.

[16] W. Gao, R.L. Robinson, K.A.M. Gasem, High-pressure solubilities of hydrogen, nitrogen, and carbon monoxide in dodecane from 344 to 410 K at pressures to 13.2 MPa, Journal of Chemical and Engineering Data. 44 (1999) 130–132. https://doi.org/10.1021/je9801664.

[17] T. Garcia-Cordova, D.N. Justo-García, B.E. García-Flores, F. Garcia-Sanchez, Vapor-Liquid Equilibrium Data for the Nitrogen and Dodecane System at Temperatures from (344 to 593) K and at Pressures up to 60 MPa, Journal of Chemical and Engineering Data. 56 (2011) 1555–1564. https://doi.org/10.1021/je1012372.

[18] D.Y. Peng, D.B. Robinson, A New Two-Constant Equation of State, Industrial and Engineering Chemistry Fundamentals. 15 (1976) 59–64. https://doi.org/10.1021/i160057a011.

[19] J.S. Lopez-Echeverry, S. Reif-Acherman, E. Araujo-Lopez, Peng-Robinson equation of state: 40 years through cubics, Fluid Phase Equilibria. 447 (2017) 39–71.

[20] S.E.K. Fateen, M.M. Khalil, A.O. Elnabawy, Semi-empirical correlation for binary interaction parameters of the Peng-Robinson equation of state with the van der Waals mixing rules for the prediction of high-pressure vapor-liquid equilibrium, Journal of Advanced Research. 4 (2013) 137–145. https://doi.org/10.1016/j.jare.2012.03.004.

[21] F. Mohammed, M. Qasim, A. Elamir, N.A. Darwish, Generalized binary interaction parameters for hydrogen-heavy-n-alkane systems using Peng–Robinson equation of state, Chemical Engineering Communications. 205 (2018) 1226–1238. https://doi.org/10.1080/00986445.2018.1442333.

[22] A.M. Abudour, S.A. Mohammad, R.L. Robinson, K.A.M. Gasem, Generalized binary interaction parameters for the Peng-Robinson equation of state, Fluid Phase Equilibria. 383 (2014) 156–173. https://doi.org/10.1016/j.fluid.2014.10.006.

[23] S. Mohanty, Estimation of vapour liquid equilibria of binary systems, carbon dioxide-ethyl caproate, ethyl caprylate and ethyl caprate using artificial neural networks, Fluid Phase Equilibria. 235 (2005) 92–98. https://doi.org/10.1016/j.fluid.2005.07.003.

[24] R. Petersen, A. Fredenslund, P. Rasmussen, Artificial neural networks as a predictive tool for vapor-liquid equilibrium, Computers and Chemical Engineering. 18 (1994) S63–S67. https://doi.org/10.1016/0098-1354(94)80011-1.

[25] R. Sharma, D. Singhal, R. Ghosh, A. Dwivedi, Potential applications of artificial neural networks to thermodynamics: Vapor-liquid equilibrium predictions, Computers and Chemical Engineering. 23 (1999) 385–390. https://doi.org/10.1016/S0098-1354(98)00281-6.

[26] S. Ganguly, Prediction of VLE data using radial basis function network, Computers and Chemical Engineering. 27 (2003) 1445–1454. https://doi.org/10.1016/S0098-1354(03)00068-1.

[27] S. Mohanty, Estimation of vapour liquid equilibria for the system carbon dioxide-difluoromethane using artificial neural networks, International Journal of Refrigeration. 29 (2006) 243–249. https://doi.org/10.1016/j.ijrefrig.2005.05.007.

[28] H. Ghanadzadeh, H. Ahmadifar, Estimation of (vapour + liquid) equilibrium of binary systems (tert-butanol + 2-ethyl-1-hexanol) and (n-butanol + 2-ethyl-1-hexanol) using an artificial neural network, Journal of Chemical Thermodynamics. 40 (2008) 1152–1156. https://doi.org/10.1016/j.jct.2008.02.011.

[29] W.A. Habiballah, R.A. Startzman, M.A. Barrufet, Use of Neural Networks for Prediction of Vapor/Liquid Equilibrium K-Values for Light-Hydrocarbon Mixtures, SPE Reservoir Engineering. 11 (2007) 121–126. https://doi.org/10.2118/28597-pa.

[30] R. Abedini, I. Zanganeh, M. Mohagheghian, Simulation and estimation of vapor-liquid equilibrium for asymmetric binary systems (CO 2-Alcohols) using artificial neural network, Journal of Phase Equilibria and Diffusion. 32 (2011) 105–114. https://doi.org/10.1007/s11669-011-9851-8.

[31] H. Karimi, F. Yousefi, Correlation of Vapour Liquid Equilibria of Binary Mixtures Using Artificial Neural Networks, Chinese Journal of Chemical Engineering. 15 (2007) 765–771. https://doi.org/10.1016/S1004-9541(07)60160-8.

[32] R. Sharma, D. Singhal, R. Ghosh, A. Dwivedi, Potential Applications of Artificial Neural Networks to Thermodynamics, Computers and Chemical Engineering. 23 (2013) 49–59. https://doi.org/10.1201/b13115-7.

[33] P. Rai, G.C. Majumdar, S. DasGupta, S. De, Prediction of the viscosity of clarified fruit juice using artificial neural network: A combined effect of concentration and temperature, Journal of Food Engineering. 68 (2005) 527–533. https://doi.org/10.1016/j.jfoodeng.2004.07.003.

[34] C. Bouchard, B.P.A. Granjean, A neural network correlation for the variation of viscosity of sucrose aqueous solutions with temperature and concentration, LWT - Food Science and Technology. 28 (1995) 157–159. https://doi.org/10.1016/S0023-6438(95)80029-8.

[35] S. Laugier, D. Richon, Use of artificial neural networks for calculating derived thermodynamic quantities from volumetric property data, Fluid Phase Equilibria. 210 (2003) 247–255. https://doi.org/10.1016/S0378-3812(03)00172-9.

[36] S. Potukuchi, A.S. Wexler, Predicting vapor pressures using neural networks, Atmospheric Environment. 31 (1997) 741–753. https://doi.org/10.1016/S1352-2310(96)00203-8.

[37] S.S. Sablani, O.D. Baik, M. Marcotte, Neural networks for predicting thermal conductivity of bakery products, Journal of Food Engineering. 52 (2002) 299–304. https://doi.org/10.1016/S0260-8774(01)00119-4.

[38] S. Urata, A. Takada, J. Murata, T. Hiaki, A. Sekiya, Prediction of vapor-liquid equilibrium for binary systems containing HFEs by using artificial neural network, Fluid Phase Equilibria. 199 (2002) 63–78. https://doi.org/10.1016/S0378-3812(01)00814-7.

[39] M. Mesbah, E. Soroush, V. Azari, M. Lee, A. Bahadori, S. Habibnia, Vapor liquid equilibrium prediction of carbon dioxide and hydrocarbon systems using LSSVM algorithm, Journal of Supercritical Fluids. 97 (2015) 256–267. https://doi.org/10.1016/j.supflu.2014.12.011.

[40] A. Roosta, J. Hekayati, J. Javanmardi, Application of artificial neural networks and genetic programming in vapor–liquid equilibrium of C 1 to C 7 alkane binary mixtures, Neural Computing and Applications. 31 (2019) 1165–1172. https://doi.org/10.1007/s00521-017-3150-1.

[41] B. Csáji, Approximation with artificial neural networks, Eotvos Lorand University, 2001. https://doi.org/10.1.1.101.2647.

[42] R. HECHT-NIELSEN, Theory of the Backpropagation Neural Network, in: Neural Networks for Perception, Academic Press, Inc., 1992: pp. 65–93. https://doi.org/10.1016/b978-0-12-741252-8.50010-8.

[43] N. Alqahtani, R.T. Armstrong, P. Mostaghimi, Deep Learning Convolutional Neural Networks to Predict Porous Media Properties, in: SPE Asia Pacific Oil and Gas Conference and Exhibition, Society of Petroleum Engineers, 2018. https://doi.org/10.2118/191906-MS.

[44] N. Srisutthiyakorn, Deep learning methods for predicting permeability from 2-D/3-D binary segmented images, in: SEG Technical Program Expanded Abstracts, Society of Exploration Geophysicists, 2016: pp. 3042–3046. https://doi.org/10.1190/segam2016-13972613.1.

[45] R. Eskandarpour, A. Khodaei, Machine Learning Based Power Grid Outage Prediction in Response to Extreme Events, IEEE Transactions on Power Systems. 32 (2017) 3315–3316. https://doi.org/10.1109/TPWRS.2016.2631895.

[46] Y. Sun, X. Fan, Q. Huang, X. Li, R. Huang, T. Yin, G. Lin, Local Feature Sufficiency Exploration for Predicting Security-Constrained Generation Dispatch in Multi-area Power Systems, in: 17th IEEE International Conference on Machine Learning and Applications, Institute of Electrical and Electronics Engineers Inc., 2018: pp. 1283–1289. https://doi.org/10.1109/ICMLA.2018.00208.

[47] S. Sadiqbatcha, Y. Zhao, J. Zhang, H. Amrouch, J. Henkel, S.X.D. Tan, Machine Learning Based Online Full-Chip Heatmap Estimation, in: Proceedings of the Asia and South Pacific Design Automation Conference, ASP-DAC, Institute of Electrical and Electronics Engineers Inc., 2020: pp. 229–234. https://doi.org/10.1109/ASP-DAC47756.2020.9045204.

[48] J. Yang, W. Wang, G. Lin, Q. Li, Y. Sun, Y. Sun, Infrared Thermal Imaging-Based Crack Detection Using Deep Learning, IEEE Access. 7 (2019) 182060–182077. https://doi.org/10.1109/ACCESS.2019.2958264.

[49] NIST Chemistry WebBook, (n.d.). https://webbook.nist.gov/chemistry/.

[50] M. Wirths, Fluid-Phasengleichgewichte und kritische Erschinungen binarer Mischungen von Kohlenwasserstoffen mit Tetrafluormethan, Trifluormethan und Stickstoff zwischen 273 K und 630 K und bei Drucken bis 250 MPa, 1983.

[51] A. Azarnoosh, J.J. Mcketta, Vapor – liquid equilibrium in the methane -n-decane - nitrogen system, Journal of Chemical and Engineering Data. 8 (1963) 513–519.